

EFFECT OF INLET GEOMETRY ON FILM COOLING PERFORMANCE FOR GAS
TURBINE APPLICATIONS

A Thesis

by

HANLIN WANG

Submitted to the Office of Graduate and Professional Studies of
Texas A&M University
in partial fulfillment of the requirements for the degree of

MASTER OF SCIENCE

Chair of Committee,	Lesley M. Wright
Committee Members,	Je-Chin Han
	Hamn-Ching Chen
Head of Department,	Andreas A. Polycarpou

May 2021

Major Subject: Mechanical Engineering

Copyright 2021 Hanlin Wang

ABSTRACT

Modern gas turbine engines require a sophisticated cooling system design to achieve higher power output and efficiency. Film cooling is an indispensable part of the turbine external cooling mechanism. In this study, systematic tests were carried out to evaluate the potential effect of non-cylindrical inlet geometries on the performance of laid back, fan-shaped film cooling holes using the steady state pressure sensitive paint (PSP) measurement technique. “Racetrack” shaped inlet geometries with aspect ratios of 2:1 and 4:1 were selected as the subjects of this study, due to their possible potential of improving the film cooling effectiveness. The outlets of the tested film cooling holes share the same geometric parameters of a fan-shaped hole design studied in open literature, while the inlet geometry varies. The coolant flow conditions range from blowing ratios of $M=0.3-1.5$ and density ratios $DR=1$ and 2 . The mainstream turbulence intensity is fixed at 6% . Results show that the shaped inlets can provide a higher area-averaged film cooling effectiveness, η , over the traditional cylindrical inlet design using the same amount of coolant, but the performance varies with flow conditions. For the 2:1 inlet, an advantage of 20% higher η could be maintained for $DR=1$, while for $DR=2$ this advantage is reduced to 10% . For the 4:1 inlet, when the coolant momentum flux ratio $I < 0.5$, a similar or slightly higher improvement can be obtained, but when $I > 1$, the advantage diminishes with the growing momentum flux ratio to approximately 5% at $I = 2.25$. The coolant coverage for the 2:1 inlet is better than the other two geometries downstream at higher momentum flux ratios ($I > 1$). While the 4:1 inlet enjoys a more

concentrated film coverage in regions closer to the hole ($X/D_h < 5$) when $I < 0.5$. The discharge coefficients results show that the 2:1 inlet geometry is similar to the cylindrical inlet in terms of discharge coefficients under most flow conditions. For the 4:1 inlet, its discharge coefficient is 0.02-0.04 lower than the fan-shaped holes with a cylindrical inlet under the same flow condition.

DEDICATION

This thesis is dedicated to all who provided generous and precious support for me, both mentally and materially, during these trying times.

ACKNOWLEDGEMENTS

I would like to express my genuine gratitude to my committee chair Dr. Wright, and my committee members, Dr. Han and Dr. Chen, for their guidance and support throughout this research project.

Thanks also goes to Mr. Garrick Garza in the Physics Machine Shop, who helped me prepare the necessary instruments, as well as my colleagues in our research group who provided invaluable advice and support. All Department and University faculty and staff are also to be thanked for providing the infrastructure and environment for my experience at Texas A&M University.

Finally, thanks to my family members for their care and support during these unusual times.

CONTRIBUTORS AND FUNDING SOURCES

Contributors

This work was supervised by a thesis committee consisting of Professor Lesley M. Wright (advisor) and Professor Je-Chin Han of the Department of Mechanical Engineering and Professor Hamn-Ching Chen of the Department of Civil Engineering.

The computer code used in this study for the steady state PSP measurement technique was in part based on the work of Professor Lesley M. Wright.

All other work conducted for the thesis was completed by the student independently.

Funding Sources

Graduate study was in part supported by a fellowship from Texas A&M University.

NOMENCLATURE

Nomenclature

A	Cross-sectional area of film cooling holes
ACRV	Anti-Counter Rotating Vortices
AR	Outlet-inlet cross-sectional area ratio of film cooling holes
C	Concentration
CCD	Charge-coupled device
CRV	Counter Rotating Vortices
C_d	Discharge coefficient
D_h	Hydraulic diameter of film cooling holes
DR	Density ratio
H	Height of film cooling hole cross section
I	Momentum flux ratio of coolant flow/ Emission intensity of images
IR	Emission Intensity Ratio
IR	Infrared
L	Length of film cooling holes
LED	Light-emitting diode
LIF	Laser-Induced Fluorescence
M	Blowing ratio
\dot{m}	Mass flow rate

P	Pitch of film cooling holes, Pressure
PIV	Particle Image Velocimetry
PSP	Pressure Sensitive Paint
PR	Pressure Ratio
S	Slot width/equivalent slot width of a set of discrete holes
SLA	Stereolithography
T	Temperature
TIT	Turbine Inlet Temperature
U	Uncertainty
v	Velocity
W	Width of film cooling hole cross section
X	Streamwise distance from the trailing edge of the film cooling holes
Y	Lateral distance from the centerline of the film cooling holes
η	Film cooling effectiveness
θ	Inclination angle of film cooling holes
ξ	Non-dimensional geometric parameter in the heat sink model of two-dimensional incompressible film cooling
ρ	Density
φ_1	Expansion angle of fan shaped film cooling holes
φ_2	Laid-back angle of fan shaped film cooling holes

Subscripts

<i>air</i>	Images taken with LED array on and injecting air through cooling holes.
<i>area</i>	Area average
<i>aw</i>	Adiabatic wall
<i>blk</i>	Images taken with no ambient light source.
<i>c</i>	Coolant flow
<i>cal</i>	Images taken at a certain PSP calibration point.
<i>f</i>	Film
<i>in</i>	Inlet
<i>lat</i>	Laterally averaged
<i>m</i>	Expansion starting location
<i>mix</i>	Images taken with LED array on and injecting foreign gas through cooling holes.
<i>out</i>	Outlet
<i>s</i>	Static pressure
<i>t</i>	Total pressure
<i>ref</i>	Images taken with LED array on but no flow in the wind tunnel.
∞	Mainstream flow

TABLE OF CONTENTS

	Page
ABSTRACT	ii
DEDICATION	iv
ACKNOWLEDGEMENTS	v
CONTRIBUTORS AND FUNDING SOURCES.....	vi
NOMENCLATURE.....	vii
TABLE OF CONTENTS	x
LIST OF FIGURES.....	xii
LIST OF TABLES	xiv
CHAPTER I INTRODUCTION	1
CHAPTER II BACKGROUND	4
An Overview of Flat Plate Film Cooling	4
Important Parameters	4
Film Cooling Hole Geometry.....	7
Pressure Sensitive Paint (PSP) Technique	11
Objective of Current Study	13
CHAPTER III EXPERIMENTAL SETUP.....	14
Test Section Instrumentation and Testing Procedures	14
PSP Calibration	18
Film Cooling Hole Geometry.....	20
CHAPTER IV RESULTS AND DISCUSSION.....	24
Comparison with Open Literature.....	24
Detailed Film Cooling Effectiveness for Shaped holes	27
Fan-shaped holes with a Cylindrical inlet	28
Fan-shaped holes with the 2:1 aspect ratio inlet.....	32
Fan-shaped holes with the 4:1 aspect ratio inlet.....	35

Performance Comparison over the Range of Flow Conditions and Geometries	39
Blowing Ratio Effect.....	39
Density Ratio Effect	41
Inlet Geometry Effect.....	45
Film Cooling Effectiveness Uncertainty Analysis	53
Effect of Inlet Geometry on the Discharge Coefficient	56
CHAPTER V CONCLUSIONS AND FUTURE RECOMMENDATIONS	60
REFERENCES.....	63
APPENDIX A LATERAL AVERAGE EFFECTIVENESS PLOTS FOR ALL TESTS	66
APPENDIX B MATLAB® CODES	71

LIST OF FIGURES

	Page
Figure 1 Typical film cooling scheme of a high-pressure turbine blade, reprinted from the work of Han and Rallabandi [2].	2
Figure 2 Illustrations of kidney and anti-kidney vortices in (a) cylindrical holes and (b) fan-shaped holes, reprinted from the work of Haven et al. [15].	8
Figure 3 Test section design.	14
Figure 4 An illustration of the experimental setup.	16
Figure 5 An illustration of the PSP calibration setup.	18
Figure 6 PSP Calibration Curve.	20
Figure 7 Geometric definition of the shaped cooling holes investigated.	21
Figure 8 Comparison with laterally averaged effectiveness results for cylindrical holes, adapted from the study by Chen et al. [33]	26
Figure 9 Comparison with laterally averaged effectiveness results for laid-back, fan-shaped holes, adapted from the study by Chen et al. [33]	27
Figure 10 Detailed film cooling effectiveness distributions for fan-shaped holes with cylindrical inlet at DR=1.	30
Figure 11 Detailed film cooling effectiveness distributions for fan-shaped holes with cylindrical inlet at DR=2.	31
Figure 12 Detailed film cooling effectiveness distributions for fan-shaped holes with the 2:1 aspect ratio inlet at DR=1.	33
Figure 13 Detailed film cooling effectiveness distributions for fan-shaped holes with the 2:1 aspect ratio inlet at DR=2.	34
Figure 14 Detailed film cooling effectiveness distributions for fan-shaped holes with the 4:1 aspect ratio inlet at DR=1.	37
Figure 15 Detailed film cooling effectiveness distributions for fan-shaped holes with the 4:1 aspect ratio inlet at DR=2.	38

Figure 16 Effect of blowing ratio on the laterally averaged film cooling effectiveness. .	40
Figure 17 Effect of density ratio on the laterally averaged film cooling effectiveness for holes for shaped holes with a cylindrical inlet.	42
Figure 18 Effect of density ratio on the laterally averaged film cooling effectiveness for shaped holes with the 2:1 inlet.	43
Figure 19 Effect of density ratio on the laterally averaged film cooling effectiveness for shaped holes with the 4:1 inlet.	44
Figure 20 Effect of inlet geometry on the laterally averaged film cooling effectiveness at DR=1.0, with predicting correlations as comparison.	48
Figure 21 Effect of inlet geometry on the laterally averaged film cooling effectiveness at DR=2.0, with predicting correlations as comparison.	49
Figure 22 Area averaged effectiveness of the same area of interest in terms of momentum flux ratio.	51
Figure 23 Uncertainty of the film cooling effectiveness for 2:1 inlet, DR=1, M=1.5. (a)absolute uncertainty (b)relative uncertainty.	54
Figure 24 Film cooling effectiveness, the absolute and relative uncertainty along the centerline of the test section for DR=1, M=1.5 test of holes with the 2:1 inlet.	55
Figure 25 The variation of discharge coefficient with momentum flux ratio.	57
Figure 26 The variation of discharge coefficient with coolant-mainstream pressure ratio.	58

LIST OF TABLES

	Page
Table 1 Flow conditions investigated.....	21
Table 2 The geometric parameters of the film cooling hole designs investigated.	22
Table 3 Top and cross-sectional views of the film cooling holes investigated.	23
Table 4 Geometric and flow parameters of current study and adapted from Chen et al. [33].....	25
Table 5 Dimensions of the investigated area of detailed effectiveness distributions.....	28

CHAPTER I

INTRODUCTION

Since its invention in the 1930s, the gas turbine has undergone decades of improvement in design and manufacturing and become one of the most widely used power plants for aircraft propulsion and power generation. Thermodynamics dictates that to achieve a high efficiency and power output, the temperature of the heating process in the Brayton cycle should be as high as possible. The turbine inlet temperature (TIT) of modern, high-performance aircraft engines can reach 2000K during take-off, while advanced land-based power generation turbines can have a maximum TIT of over 1850K [1]. In future applications, the introduction of hydrogen fuels may further increase the gas temperature to a higher level.

Modern gas turbine engines require a sophisticated turbine cooling system to protect turbine airfoils and endwalls from the hot gas with a temperature well above the maximum tolerable temperature of the turbine material. At the same time, bleeding cooling air from the final stage compressors contradicts the goal of increasing engine core shaft power output. Thus, more efficient cooling schemes must be designed to meet the requirements of more reliable and more powerful gas turbine engines.

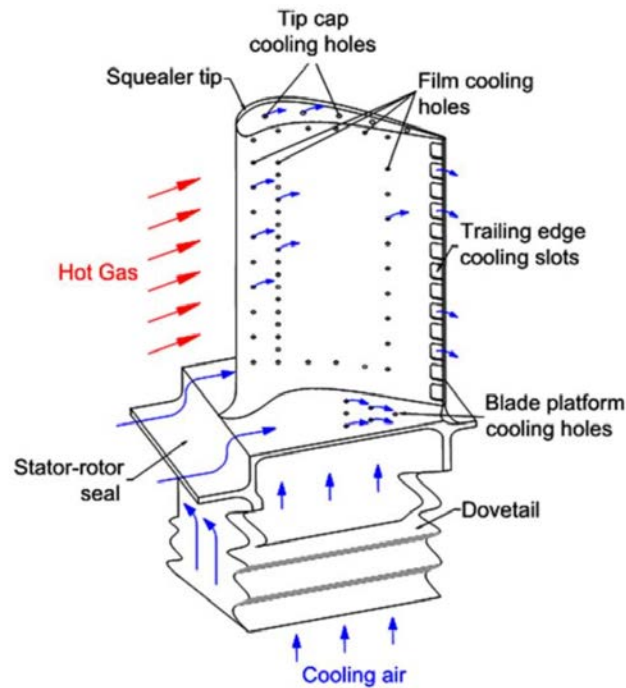


Figure 1 Typical film cooling scheme of a high-pressure turbine blade, reprinted from the work of Han and Rallabandi [2].

Film cooling has been an indispensable part of modern turbine external cooling design since its introduction. Figure 1 shows a typical external cooling design of a high pressure turbine blade, featuring multiple film cooling holes at different locations of the blade. As depicted by the definition given by Goldstein [3], film cooling is an external cooling technique which introduces a secondary fluid (in gas turbines, extracted air from the compressor stages is the most common coolant) at one or more discrete locations along the surface. The film cooling effectiveness $\eta = \frac{T_{\infty} - T_f}{T_{\infty} - T_c}$ is used to quantify how much the gas temperature near the surface is lowered by the injected coolant. The geometry and arrangement of the cooling holes, as well as the properties of the coolant and the mainstream flow, are the major influencing factors of film cooling effectiveness.

Among these, the geometry of the cooling holes has evolved from simple cylindrical holes into holes with shaped outlet sections, greatly improving the film cooling performance. The geometry of the internal passage of the film cooling hole near the inlet, however, has received less attention by researchers and is the focus of this study. Flat plate film cooling research is a low-cost approach to reveal the fundamental characteristics of film cooling and will be used in this investigation.

In this study, a steady state Pressure Sensitive Paint (PSP) technique is used to measure detailed film cooling effectiveness from shaped cooling holes with different internal passage geometries over a flat plate. The cooling holes have an identical cross-sectional area to maintain the same coolant mass flow. The variables include density ratio, blowing ratio and hole geometry. The results are compared with results of traditional inlet designs.

CHAPTER II

BACKGROUND

In this chapter, the background of this investigation is presented in two major sections, including an overview of flat plate film cooling and the introduction of PSP measurement technique.

An Overview of Flat Plate Film Cooling

According to Bogard and Thole [4], factors which can significantly affect film-cooling performance fall into three categories: coolant/mainstream flow conditions, hole geometry and airfoil geometry. Although the airfoils in an actual gas turbine are curved, preliminary investigations on the cooling flow over a flat surface can provide useful insights for how specific parameters will affect flow and heat transfer characteristics over complex shaped geometries. As Han et al. [5] stated, flat-surface film cooling is a cost-effective way to investigate the effects of individual parameters.

Important Parameters

Decades of research in the field of gas turbine film cooling has resulted in significant improvement of film cooling designs and met the growing demand in gas turbine cooling with ever-increasing power density of the engines. Goldstein et al. [3, 6] laid fundamental groundwork for film cooling and introduced parameters depicting the flow characteristics and effectiveness of a film cooling design.

The film cooling effectiveness as well as several important parameters and their impact on film cooling effectiveness are defined below:

Film cooling effectiveness, η

Film cooling effectiveness, η , represents how much the film can reduce the near surface temperature, compared with the temperature difference of the mainstream and coolant gases. It is defined in equation (1):

$$\eta = \frac{T_{\infty} - T_f}{T_{\infty} - T_c} \approx \frac{T_{\infty} - T_{aw}}{T_{\infty} - T_c} \quad (1)$$

Where T_{∞} is mainstream gas temperature, T_f is film temperature, T_{aw} is adiabatic wall temperature and T_c is coolant temperature. In actual experiments, T_f is relatively difficult to obtain, thus the adiabatic wall temperature T_{aw} is commonly used, by assuming the heat loss through the wall is zero. However, perfect insulation only exists on paper, thus a separate experiment will be needed to evaluate the impact of heat loss through the wall in heat transfer based experiments.

Density Ratio, DR

The density ratio, DR , reflects the density difference of coolant and mainstream flow due to a massive temperature difference under real engine conditions. It is defined in equation (2):

$$DR = \frac{\rho_c}{\rho_{\infty}} \quad (2)$$

Where ρ_c and ρ_{∞} are the density of the coolant and mainstream flows. Denser coolant tends to remain closer to the coolant, which would result in a higher film cooling effectiveness, as studied by Petersen et al. [7]. In a more recent investigation, Johnson et

al. [8] used more advanced measurement techniques of PSP and PIV to illustrate the effect of density ratio in a more detailed manner for cylindrical holes.

Blowing Ratio, M

Blowing ratio, M , represents the mass flux ratio between the coolant and mainstream. It is defined in equation (3):

$$M = \frac{\rho_c v_c}{\rho_\infty v_\infty} \quad (3)$$

Where ρ_c and ρ_∞ are the density of the coolant and mainstream flow; v_c and v_∞ are the velocity of the coolant and mainstream flow.

For the same cooling hole geometry, film cooling effectiveness generally increases as the blowing ratio increases. However, at a specific blowing ratio, depending on the geometry of the hole and density of the coolant, the momentum of the coolant becomes too high to keep it close to the surface. Further increasing the blowing ratio decreases the effectiveness. This phenomenon is referred to as “lift-off effect” [5].

Momentum Flux Ratio, I

The momentum flux ratio, I , represents the momentum flux ratio between the coolant and mainstream. It is defined in equation (4):

$$I = \frac{\rho_c v_c^2}{\rho_\infty v_\infty^2} = \frac{M^2}{DR} \quad (4)$$

Where ρ_c and ρ_∞ are the density of the coolant and mainstream flow, v_c and v_∞ are the velocity of the coolant and mainstream flow. It is more useful in evaluating the

cases that are different in both factors, especially at higher blowing ratios, when the momentum of the coolant is the more dominant factor influencing the effectiveness.

Free Stream Turbulence Intensity, $Tu\%$

Free stream turbulence intensity is the ratio of average velocity fluctuation, u' , to the mean velocity, \bar{u} , of a turbulent flow. It is defined in equation (5):

$$Tu\% = \frac{u'}{\bar{u}} \quad (5)$$

The nature of the mainstream flow after the combustor in a real engine is highly turbulent. Turbulence intensity reflects the scale of vortices existing in the flow. It can reach 20% at the first stage vane inlet under actual engine conditions. High turbulence intensity would decrease the effect of coolant injection as the coolant would be more likely to mix with the mainstream flow. As a result, film cooling effectiveness is reduced with high mainstream turbulence intensity, according to Bons et al. [9]. More recently, Schroeder and Thole [10] used IR thermal imaging and PIV measuring techniques to present a detailed flow field and effectiveness distribution under high and low turbulence intensities for a shaped hole geometry.

Film Cooling Hole Geometry

Extensive research shows that the geometry of the film cooling holes has a significant impact on film cooling effectiveness at different ranges of blowing ratio and coolant density. The advancement in manufacturing techniques allows more sophisticated cooling hole designs to be adopted into the engines. A well-designed

geometry can greatly improve the film cooling effectiveness in cooling schemes with similar flow parameters, especially at regions immediately downstream of the holes.

Goldstein et al. [6] made pioneering contributions in discovering the potential of fan-shaped cooling holes to improve the overall effectiveness and lateral film coverage over traditional cylindrical holes. This can be reinforced by works from Gritsch et al. [11] and Wright et al. [12] with more detailed results. Bunker [13] made an extensive review of the works on shaped holes and pointed out shaped holes still have the potential to be further improved in performance. By the definition of Bunker [13], the shaped film hole contains some initial round entry length that acts as the metering or throat section, followed by an expanded diffuser-type exit intended to spread the coolant flow laterally and/or onto the surface. Colban et al. [14] gathered a substantial dataset of shaped film cooling hole designs and their performances and developed a predicting correlation for the performance of shaped film cooling holes.

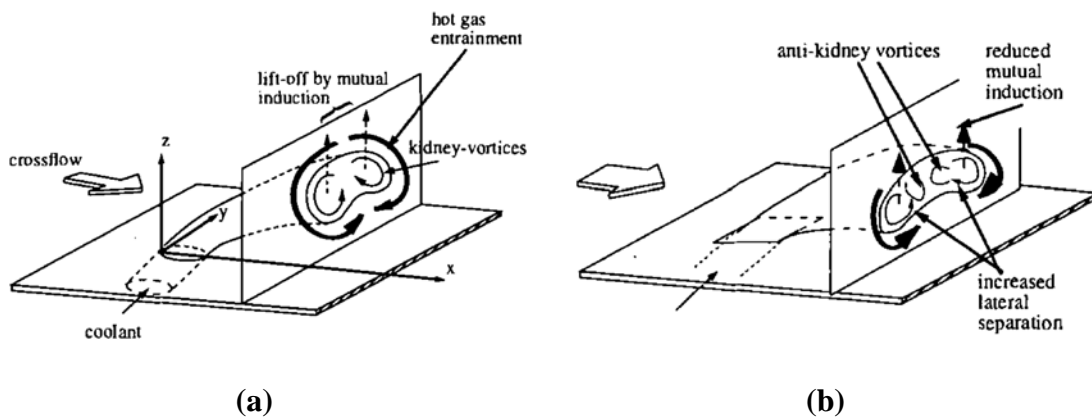


Figure 2 Illustrations of kidney and anti-kidney vortices in (a) cylindrical holes and (b) fan-shaped holes, reprinted from the work of Haven et al. [15].

Recent studies show more effort of the researchers to investigate new-concept geometries and improve existing designs. Lee and Kim [16] computationally optimized

the geometry of traditional fan-shaped holes and achieved a 34% increase in averaged effectiveness. Heidmann and Ekkad [17] put forward a new cooling concept called antivortex cooling, with the phenomena of counter rotating vortices (CRV) discovered by Haven et al. [15]. By introducing holes which generate a pair of vortices counteracting the influence of the counter-rotating kidney-shaped vortices depicted in Figure 2, the lift-off and separation effect of the high momentum coolant jets can be weakened, thus improving film cooling effectiveness. Kusterer et al. [18, 19] made further investigation into this concept and created a new type of cooling holes which specifically designed to generate anti-counter-rotating-vortices (ACRV) to achieve better performance than traditional fan-shaped holes. Kawabachi et al. [20, 21] developed such a concept in parallel and used a revised upstream geometry to generate such anti-vortices and achieved a similar improvement effect. Lu et al. [22] and Wayne and Bogard [23] investigated the combination of trenches and cylindrical holes to achieve comparable or better performance since it is a more cost-friendly option to manufacture and maintain compared to fan-shaped holes.

Compared with more numerous studies of the outlet geometries, the geometry of the cooling flow passage and the inlet has received less attention. However, the potential effect of inlet geometry cannot be omitted. Haven and Kurosaka [24] investigated the kidney vortices in a cross flow cooling flow using PIV and LIF methods, which revealed that the jets from the high-aspect-ratio holes, with increased separation distance between the sidewall vortices, stays attached to the surface even for higher blowing ratios. Rhee et al. [25] investigated the performance of rectangular-shaped inlets both experimentally

and numerically, and showed it is more effective than traditional cylindrical holes.

Takahashi et al. [26] used a thermocouple measurement technique to evaluate a series of non-cylindrical-shaped straight holes and revealed there are shapes that are superior to cylindrical holes and possess the potential to be further improved in performance.

Watson et al. [27] investigated a novel shaped inlet that resembles a slot for laid-back, fan-shaped holes using PSP technique and found there should be an optimal inlet

geometry to maximize the effectiveness. Ullah et al. [28] investigated the effectiveness of an annulus cooling hole outlet design and a projectile-trajectory-shaped inlet profile.

Results showed slot holes with a projectile trajectory flow path achieved 30-40%

improvement in effectiveness over traditional linear flow path. In a most recent study by

Yu et al. [29], researchers designed a diffusion-slot hole and used PSP technique to show a promising performance improvement over traditional fan-shaped holes in end wall film cooling, especially at high blowing ratios.

These studies prompted the inlet geometry can be further optimized to enhance cooling performance of a shaped hole. The results from these studies point to an inlet geometry that has a larger spanwise dimension (aspect ratio larger than 1:1) tends to have better performance over ones with a cylindrical inlet. Hence in this study, three types of laid-back, fan-shaped holes with the same inlet and outlet cross-sectional area but with different aspect ratios are studied to show the possible relation between the inlet geometry and the performance of shaped cooling holes.

Pressure Sensitive Paint (PSP) Technique

The PSP measurement technique primarily utilizes the photoluminescence property of the PSP paint and a mass transfer analogy. Although pressure sensitive paint itself was invented decades ago, the PSP technique in the field of turbine film cooling has been relatively implemented more recently compared with traditional heat transfer measurement techniques. It was first introduced by Zhang and Fox [30] and further assessed by Wright et al. [31] to show the potential of this measurement technique. In the work from Han and Rallabandi [2], the theoretical basis of this technique is presented in detail.

The primary advantage of the PSP technique in film cooling studies is that it uses a mass transfer analogy to accurately measure detailed distributions of the film cooling effectiveness over an area without tackling the problem of heat loss and heat transfer through the wall, as encountered in heat transfer techniques. However, the PSP technique alone cannot measure the heat transfer coefficient, so it should be coupled with heat transfer experiments to reveal the full picture of the performance of a certain film cooling scheme.

The principle of the PSP technique is based upon the “oxygen quenching” property of the PSP paint. When excited by a certain wavelength of light, PSP paint molecules will emit photons with a longer wavelength. The emission intensity of the molecules is inversely correlated with the local oxygen partial pressure. The mass transfer analogy implies thermal diffusion is analogous to mass diffusion. The

temperature is replaced by mass concentration in the defining equation of the film cooling effectiveness, which can be expressed in the following:

$$\eta = \frac{T_{\infty} - T_f}{T_{\infty} - T_c} = \frac{C_{\infty} - C_f}{C_{\infty} - C_c} = \frac{P(O_2)_{air} - P(O_2)_{mix}}{P(O_2)_{air}} \quad (6)$$

Where C_{∞} , C_f and C_c are the concentrations of oxygen in the mainstream flow, the film and coolant, respectively. If a foreign gas with no oxygen content is used and the surface is completely purged in the gas, the term C_c is reduced to zero. From Dalton's law of partial pressure, given an ideal gas, the concentration is equal to the partial pressure. Through an independent calibration process, the partial pressure of the oxygen can be related to the emission intensity ratio obtained from the images:

$$PR = \frac{P(O_2)}{P(O_2)_{ref}} = Fn \left(\frac{I_{ref} - I_{blk}}{I_{cal} - I_{blk}} \right) = Fn(IR) \quad (7)$$

Where a reference image is taken when the excitation light is on at ambient pressure, from which the intensity I_{ref} is extracted. I_{blk} is the intensity when all ambient light is turned off and I_{cal} is the intensity when the pressure is reduced with the excitation light source is on.

In this manner, the partial pressure of oxygen, and subsequently the film cooling effectiveness, can be obtained by measuring the emission intensity of the PSP paint. If the density of the foreign gas is not equivalent to air, the film cooling effectiveness needs to be adjusted by the density ratio DR of foreign gas to air, according to Charbonnier et al. [32]:

$$\eta = 1 - \frac{1}{(PR_{air}/PR_{mix}-1) \cdot DR + 1} \quad (8)$$

As there is no heat transfer process involved, the PSP technique does not need to take heat loss through the wall into consideration, which could become an important factor that needs to be included in steady-state heat transfer experiments. When compared with more traditional mass transfer techniques, like foreign gas sampling, the PSP technique has much greater spatial resolution and can provide detailed distributions of film cooling effectiveness which the former can only provide data on discrete sampling points.

Objective of Current Study

The primary goal of this research is to use the PSP measurement technique to obtain detailed effectiveness distributions of simple cylindrical holes and fan-shaped cooling holes of different inlet geometries. The variables of flow parameters include density ratio and blowing/momentum flux ratio. Based on the data obtained in the experiments, a cross-comparison is made to assess the impact of the inlet geometry on the performance of a fan-shaped cooling hole. These investigations aim to complement a less-studied area of academic research on turbine film cooling and provide useful insights for the designs of real turbine cooling schemes, ultimately contributing to the development of more powerful and more efficient gas turbines.

CHAPTER III
EXPERIMENTAL SETUP

In this chapter, the experimental setup of this investigation is presented in three categories, including the instrumentation of the test section and testing procedures, PSP calibration and the geometries investigated.

Test Section Instrumentation and Testing Procedures

In this investigation, the same low-speed, suction-type wind tunnel used by Chen et al. [33] and Rallabandi et al. [34] is used to sustain the mainstream flow. The cross section of the wind tunnel channel is a rectangle with a dimension $30.48 \times 15.24\text{cm}$. The mean velocity of the flow is maintained at 21.6 m/s. A turbulence grid is used to generate flows with a turbulence intensity of 6%.

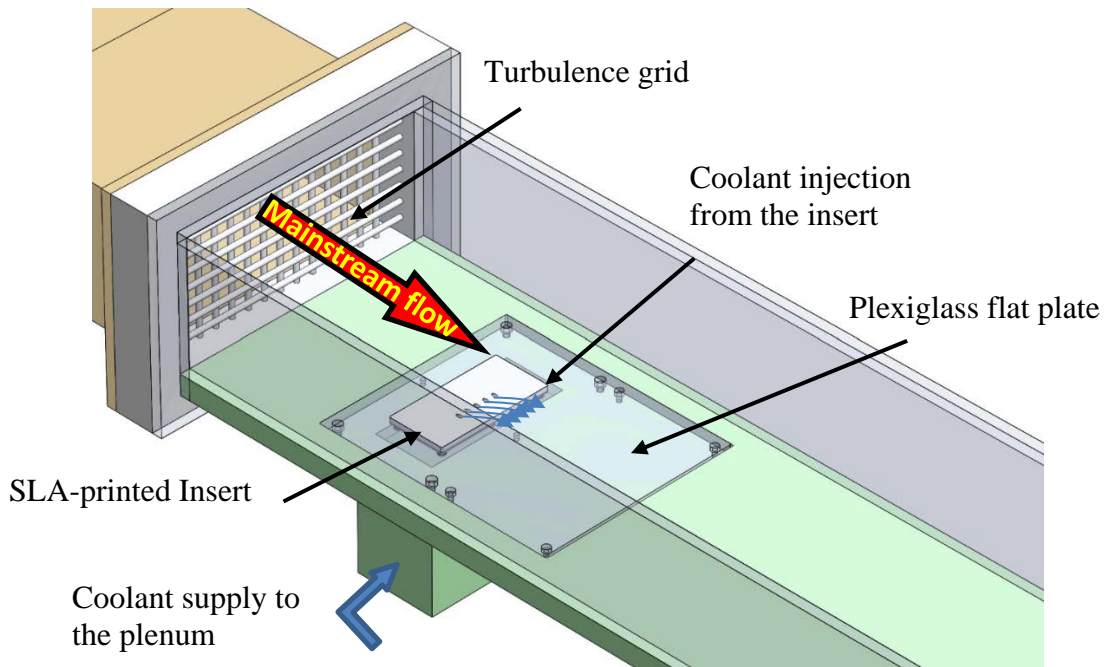


Figure 3 Test section design.

As depicted in Figure 3, the test section has a plenum which is connected to compressed air and foreign gas supplies. The top of the plenum is covered with the flat plate to be tested. The plate is made of plexiglass and there is a slot on it to insert the SLA (Stereolithography) additively-manufactured film cooling hole section. The manufacturing of the insert is completed by Protolabs using Accura Xtreme White material. After inserting the cooling holes, the gap between the insert and the plate is eliminated by applying silicone clay and sanding to maintain the continuity of the surface. Then the plate is sprayed with a layer of black paint to serve as base coating. Finally, the PSP paint is sprayed evenly on the area of interest around and downstream of the holes.

During tests, a CCD camera, which captures 16-bit gray-scale images with a resolution of 320×240 pixels, is connected to a PC for recording images using CAMWARE software during testing, together with a 400nm wavelength LED light source to excite the PSP is installed above the testing section. The plenum is connected to a system of hoses and valves which connect the rotameters. Four rotameters purchased from Dwyer Instruments (RMC-100 series) with measuring ranges of 10-50, 20-100, 20-200 and 20-200 SCFH (ft^3/h) are used to measure the volumetric flow rate of the coolant. A 0-5 psi pressure gauge is connected to the outlet of each rotameter in order to obtain the pressure readings for adjusting the flow rate. A pitot-static tube connected with a digital manometer is used to measure the difference between the total and static pressure of the mainstream flow. The foreign gases used in this investigation

are Nitrogen ($DR \approx 1$) and 15% – 85% volumetric mixture of $SF_6 - Ar$ ($DR \approx 2$) supplied by Praxair Inc. in cylinders. The complete experiment setup is illustrated in Figure 4.

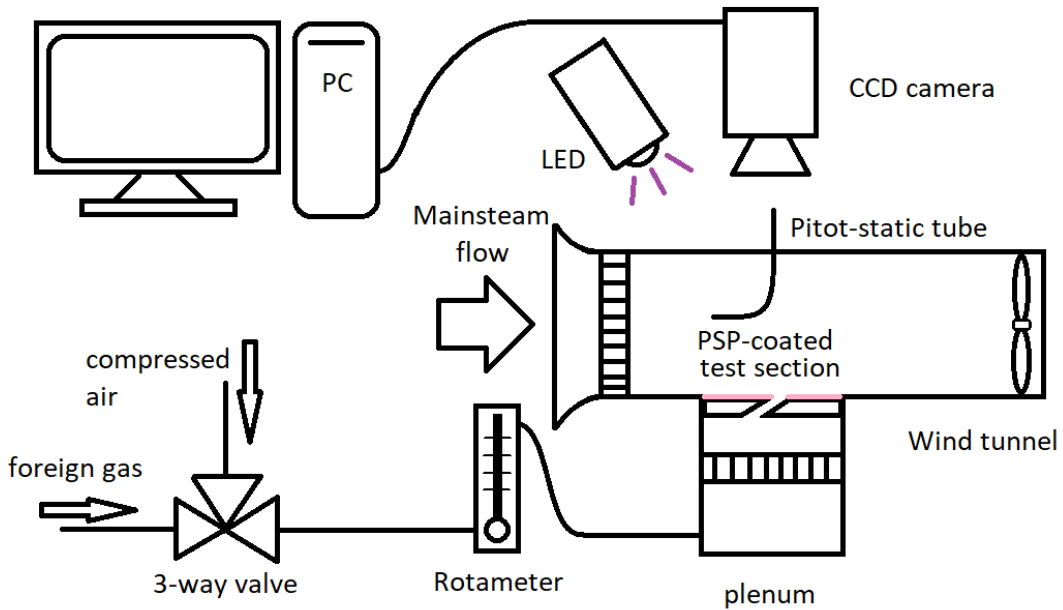


Figure 4 An illustration of the experimental setup.

The testing is completed in the following steps:

Before the testing begins, the test section is installed to the plenum, and all ambient lighting is switched off to create a dark background. The camera records the first set of 200 images as I_{blk} . Next, the LED array is turned on, and the camera records a set of 200 images as I_{ref} . Subsequently, the wind tunnel is started, a Pitot-static tube together with a digital manometer measure the difference between the total and static pressures in the tunnel. Based on local atmospheric pressure during testing and room

temperature recorded by a thermometer in the room, the equivalent pressure difference for 21.6 m/s is calculated. A sliding door is used to control the amount of airflow at the exit of the blower, which serves as the velocity controlling mechanism. After the mainstream velocity is set, actual testing begins. The cut-off valve from the compressed air source is opened, the required flow rate of air is calculated initially assuming there is no excess pressure in the flow path. Then the rotameter is adjusted to the initially calculated flow rate. Based on the reading from the pressure gauge and room temperature, a new flowrate is calculated according to an adjustment equation provided by Dwyer Inc. and the rotameter is adjusted to the newly calculated value. This process is repeated until the pressure gauge reading does not change to assure the flowrate indicated on the rotameter represents the actual flowrate. Then the LED is turned on and a set of 200 air images, in which I_{air} is recorded, is taken. After the air test is completed, coolant is switched from air to a foreign gas. The foreign gas runs through the hoses for a period of time to make sure the line is purged with the gas. Then the same procedure of recording images is applied again to take a set of 200 images to obtain I_{mix} .

To check the repeatability the data obtained in a single day's tests, for each type of gas, two sets of images are recorded. After the test is finished, another set of black and reference images are taken. Then the two sets of black, reference and mixture data are cross-paired to calculate the effectiveness results. The set of matching images with the average pressure ratio of a certain upstream area closest to zero will be selected as the recorded result, and this upstream pressure ratio will be subtracted across the entire

area of interest before making the final calculation of effectiveness to make sure the upstream effectiveness maintains at zero, as no foreign gas should exist in the upstream.

PSP Calibration

The apparatus for the calibration of PSP paint is illustrated in Figure 5. The chamber used for calibration consists of a stainless-steel chamber and a bolted-on plexiglass cover, a rubber O-ring serves as sealing between the cover and the chamber. A vacuum gauge with measuring increments of 5 inHg and a range of -30 to 0 inHg is connected onto a tee outlet. On one side of the tee a quick-release valve is installed, and on the other end, a vacuum pump is connected to provide the necessary negative pressure in the calibration procedure. Additional cut-off valves are installed between the pump and the chamber to more thoroughly seal the chamber to maintain relatively constant pressure in the chamber when the camera is recording images.

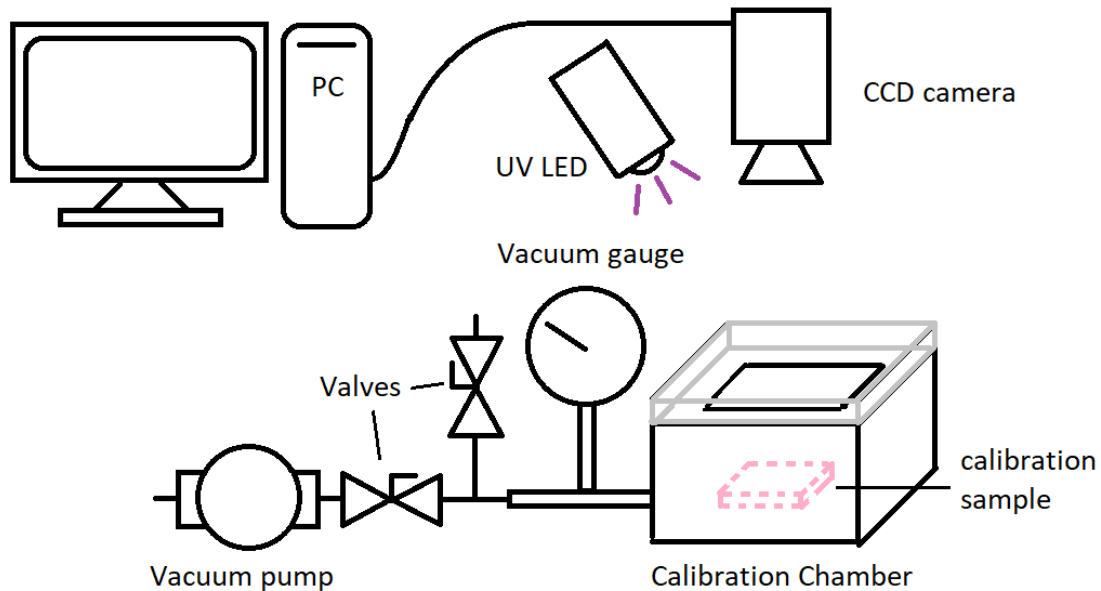


Figure 5 An illustration of the PSP calibration setup

The calibration is completed with the following procedures:

The CCD camera and LED array are put at the same distance and angle relative to the calibration chamber as they are relative to the test section during the actual experiment. After the calibration sample is put into the chamber, the cover is bolted and sealed. With all ambient lights off, a set of 200 images recording I_{black} is recorded. Then the LED is turn on, a set of images recording I_{ref} is recorded. The LED is turned off to preserve the paint when the pump is running to achieve a certain negative pressure, then the LED is turned on and the camera records the according set of images representing I .

Multiple data points are recorded, and the function between pressure ratio $PR = \frac{P(O_2)}{P(O_2)_{ref}}$, and intensity ratio $IR = \frac{I_{ref}-I_{blk}}{I_{cal}-I_{blk}}$ is curve fitted to the following 3rd order polynomial in equation (9). The calibration curve is listed as Figure 6.

$$\frac{P}{P_{ref}} = a_3 \left(\frac{I_{ref} - I_{blk}}{I_{cal} - I_{blk}} \right)^3 + a_2 \left(\frac{I_{ref} - I_{blk}}{I_{cal} - I_{blk}} \right)^2 + a_1 \left(\frac{I_{ref} - I_{blk}}{I_{cal} - I_{blk}} \right) + a_0 \quad (9)$$

Where $a_0 = -0.0287$; $a_1 = 0.6195$; $a_2 = 0.4723$; $a_3 = -0.0602$, with a curve fitting coefficient of determination $R^2 = 0.9997$.

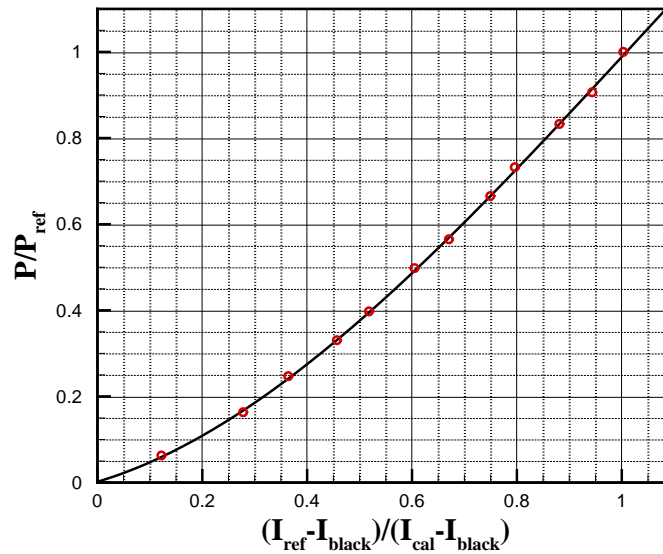


Figure 6 PSP Calibration Curve.

Film Cooling Hole Geometry

In this investigation, four geometries in total are tested with PSP. One of them is a set of standard, simple angle cylindrical holes with the inclination angle $\alpha=30^\circ$, diameter $D=4\text{mm}$ and the pitch $P = 3.75D = 15\text{mm}$. This set of round holes is meant for the validation of the instruments. The results of the cylindrical holes are compared with open literature results to make sure the experimental instruments are validated. To fully investigate the effect of inlet geometries on film cooling performance, a variety of different flow conditions are investigated for each geometry. These conditions are listed in Table 1.

The cooling hole geometries of interest are laid-back, fan-shaped holes with different inlet geometries. The principle of designing the geometry is to change the shape of the inlet cross section while maintaining the expansion angles and the cross-

sectional area at the outlet. Round, 2:1 and 4:1 aspect ratio “racetrack” shaped inlet cross sections are selected. The geometric parameters of the shaped inlet holes are defined in Figure 7 and Table 2, with all the geometries tested in this investigation listed. The top and cross-sectional views of the holes are shown in Table 3. As some of the geometries have a larger outlet width than the pitch of the cylindrical holes for benchmarking, to compare the geometries in the same manner, the pitch of the shaped holes is larger than the round hole and is kept as a constant value of 24mm, instead of varying with a fixed P/D_h ratio.

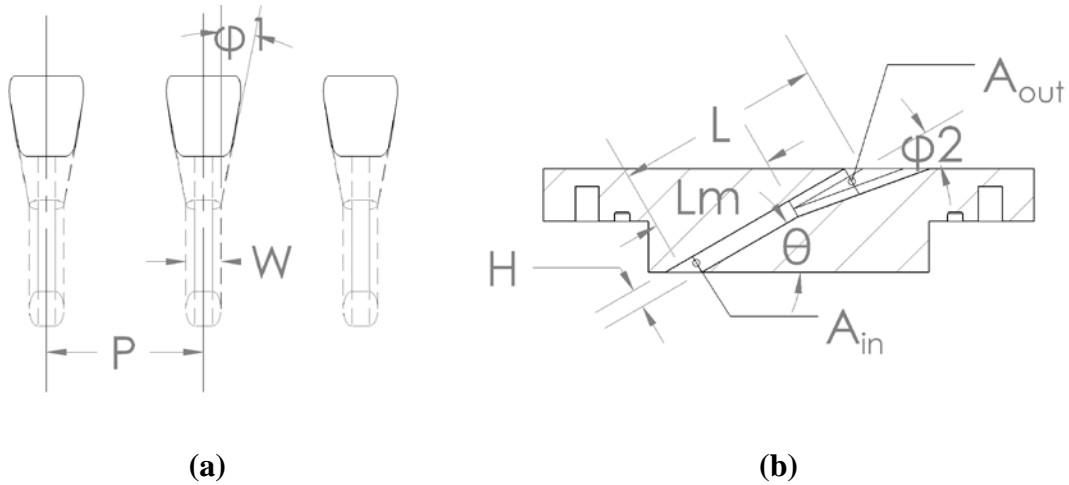


Figure 7 Geometric definition of the shaped cooling holes investigated.
(a) Top view (b) Cross-sectional view

Table 1 Flow conditions investigated.

Momentum flux ratio $I = M^2/DR$		Blowing ratio M			
		0.3	0.6	1	1.5
Density ratio DR	1	0.09	0.36	1	2.25
	2	0.045	0.18	0.5	1.125

Table 2 The geometric parameters of the film cooling hole designs investigated.

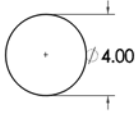
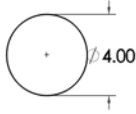
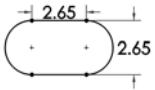
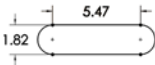
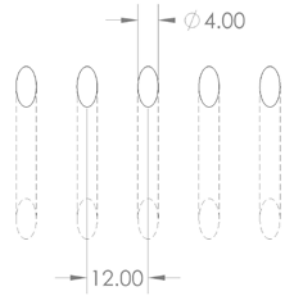
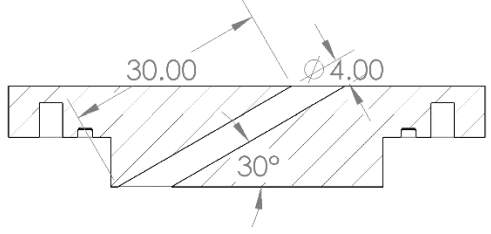
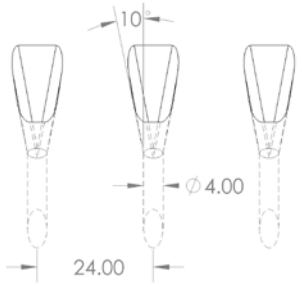
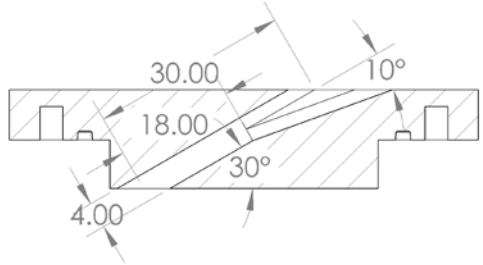
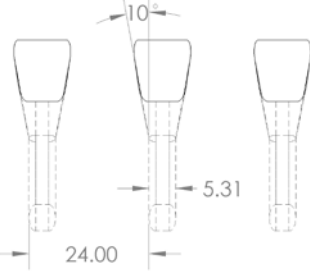
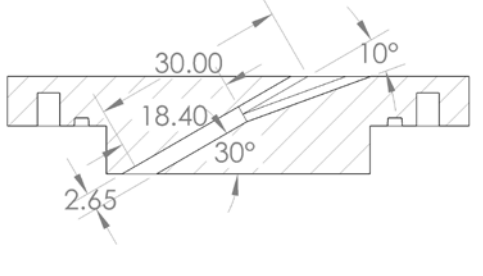
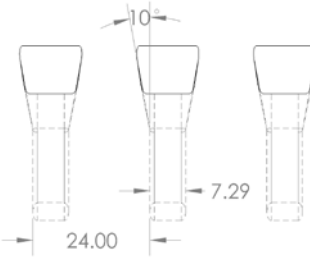
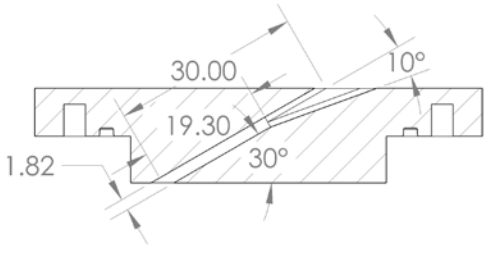
	Cylindrical hole	Cylindrical inlet fan-shaped hole	2:1 inlet fan-shaped hole	4:1 inlet fan-shaped hole
Inlet cross section shape (mm)				
Aspect ratio W/H	1: 1	1: 1	2: 1	4: 1
Number of holes	5			
θ(deg) Inclination angle	30			
φ_1(deg) Expansion angle	N/A	10		
φ_2(deg) Laid-back angle	N/A	10		
D_h(mm) Hydraulic diameter	4	4	3.685	3.0179
L(mm) Length of flow passage	30			
P/D_h Pitch-diameter ratio	3	6	6.51	7.95
A_{in}(mm²) Inlet cross-sectional area	12.6			
A_{out}(mm²) Outlet cross section area	12.56	35.16	35.10	35.14
AR Outlet-inlet area ratio	1	2.80	2.80	2.80
L/D_h Length-diameter ratio	7.5	7.5	8.14	9.94
L_m(mm) Expansion starting position of shaped outlet	N/A	18	18.4	19.3

Table 3 Top and cross-sectional views of the film cooling holes investigated.

Hole shape	Top view	Cross-sectional view
Cylindrical hole		
Round inlet fan-shaped hole		
2:1 inlet fan-shaped hole		
4:1 inlet fan-shaped hole		

CHAPTER IV

RESULTS AND DISCUSSION

This chapter presents the results of the current experimental investigation. First, the results of cylindrical holes and standard fan-shaped holes will be compared with open literature to benchmark the experimental setup. Second, the results for the shaped holes will be provided in terms of detailed effectiveness distributions and the laterally averaged effectiveness. The results will then be cross compared and discussed in terms of blowing ratio, density ratio and inlet geometry. Lastly, the uncertainty of the measurements will be presented.

Comparison with Open Literature

Cylindrical holes and fan-shaped holes with standard cylindrical inlets were tested to benchmark the experimental setup. The hole geometry and flow conditions of these benchmarking tests were kept as close as possible to those of the study by Chen et al. [33]. The exception is that the pitch of the shaped holes is 24mm instead of 15mm. The geometries are listed in Table 4. The comparisons of the laterally averaged effectiveness for cylindrical holes are plotted in Figure 8, and the comparisons of the laterally averaged effectiveness for fan-shaped holes with a cylindrical inlet are plotted in Figure 9. As the pitch of the fan-shaped holes in the current study is different from Chen et al., the laterally averaged for comparison is calculated with the same pitch ($\pm 3.75D$ or 15mm) along the y-direction. The comparisons show a satisfactory agreement with the results of Chen et al. [33]. Note that the markers in the plots only

serve the purpose of distinguishing different cases from each other and do not represent discrete datapoints of particular importance, which applies to all η_{lat} plots in this thesis.

Table 4 Geometric and flow parameters of current study and adapted from Chen et al. [33].

Geometric parameters	Current Study	Chen et al. [33]
Hole diameter D	$4mm$	
Inclination angle θ	30°	
Mainstream velocity	$21.6m/s$	
Turbulence Intensity $Tu\%$	6%	
Pitch for cylindrical holes P_{round}	$3D(12mm)$	
Pitch for fan-shaped holes P_{fan}	$3.75D(15mm)$	$6D(24mm)$
Expansion angles for fan-shaped holes φ_1, φ_2	Lateral expansion angle $\varphi_1 = 10^\circ$, Laid-back angle $\varphi_2 = 10^\circ$	
Hole length L	7.5	
Area ratio AR	2.80	2.79
Density Ratio DR	1	
Blowing Ratio M	$0.3, 0.6, 1, 1.5$	

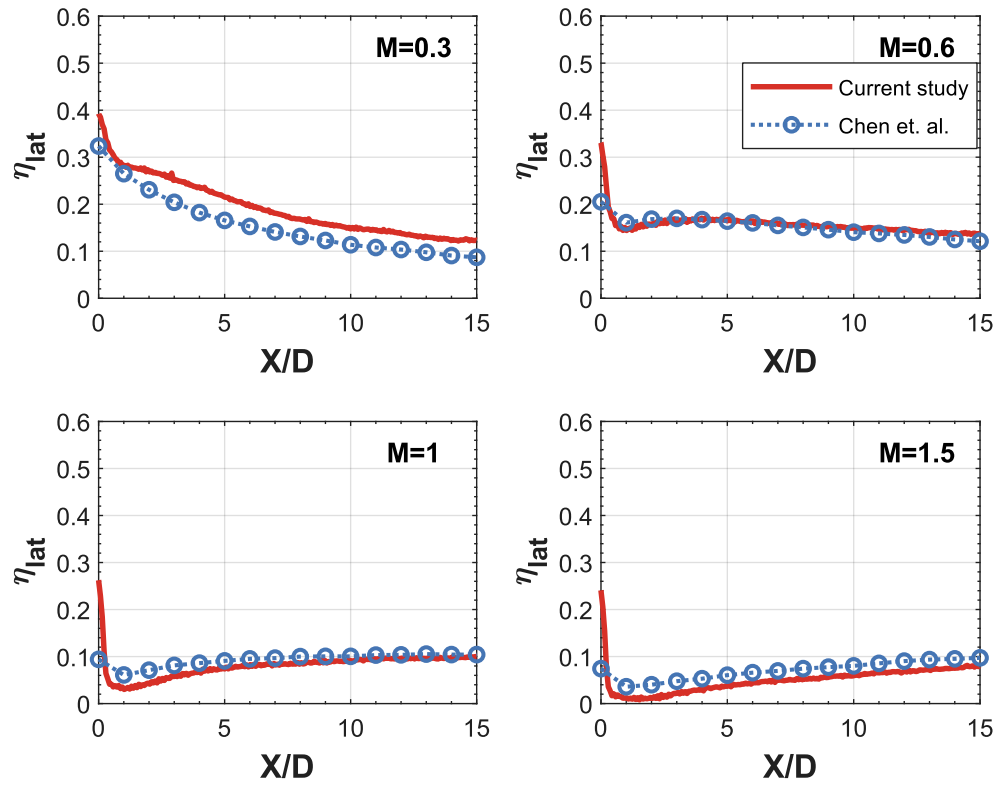


Figure 8 Comparison with laterally averaged effectiveness results for cylindrical holes, adapted from the study by Chen et al. [33]

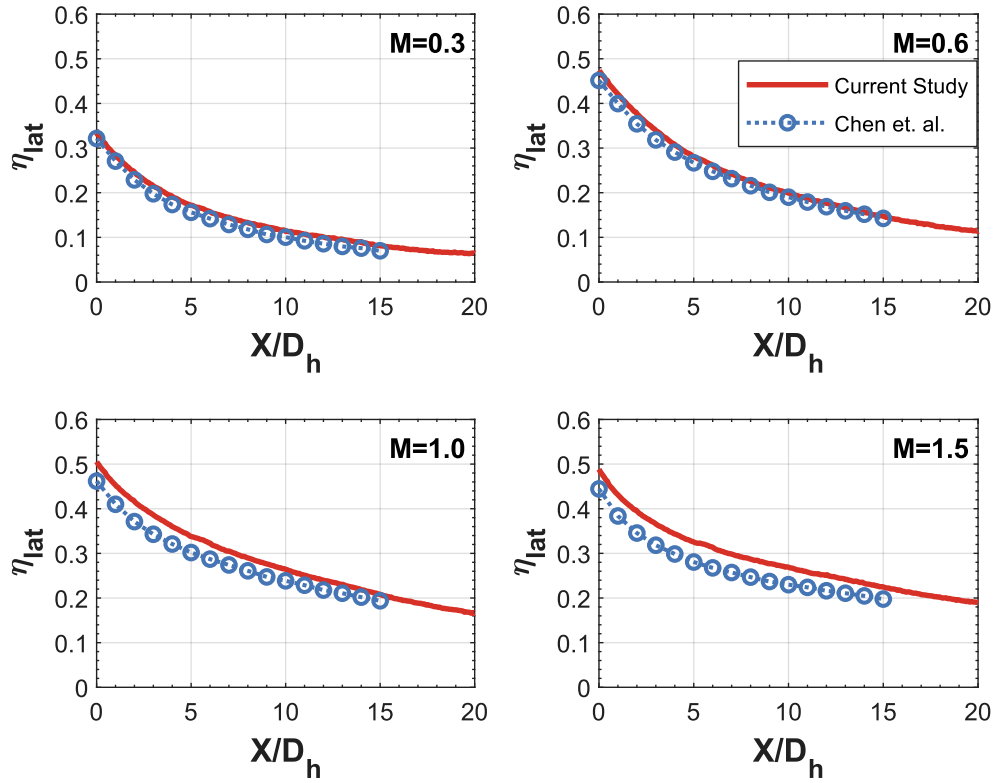


Figure 9 Comparison with laterally averaged effectiveness results for laid-back, fan-shaped holes, adapted from the study by Chen et al. [33]

Detailed Film Cooling Effectiveness for Shaped holes

The detailed film cooling effectiveness in this study was measured across the same physical area of $X \times Y = 80 \times 72mm$ downstream of the holes for all the geometries. However, as D_h of each geometry varies, the non-dimensionalized coordinates, X/D_h and Y/D_h , vary of reach geometry. To see the plots with X in physical dimensions, see Appendix A. The ranges of X/D_h and Y/D_h are listed in Table 5. The area averaged effectiveness will be calculated across the area of interest to evaluate the performance of the geometries. In the following sections, the laterally

averaged film cooling effectiveness with also be calculated with the lateral width of the area of interest.

Table 5 Dimensions of the investigated area of detailed effectiveness distributions.

Hole Geometry	Cylindrical inlet	2:1 aspect ratio inlet	4:1 aspect ratio inlet
Investigated physical area downstream of the holes $X \times Y(mm)$	80 × 72		
Inlet hydraulic diameter $D_h (mm)$	4	3.685	3.0179
Non dimensionalized streamwise length of the area X/D_h	20	21.7	26.5
Non dimensionalized lateral width of the area Y/D_h	18	19.5	23.9

Fan-shaped holes with a Cylindrical inlet

For the results of fan-shaped holes with a cylindrical inlet, the detailed film cooling effectiveness distributions for $M=0.3, 0.6, 1$ and 1.5 with $DR=1$ and $DR=2$ are plotted in Figure 10 and Figure 11, respectively. From Figure 10, it can be clearly observed that the coolant ejected from a shaped hole is able to remain attached to the surface for the range of blowing ratios. At a very low blowing ratio of $M=0.3$, the mass

flux of the coolant is so low that the majority of the coolant will be diluted by the mainstream immediately after ejection, leaving a relatively shorter trace of coolant near the surface. With the blowing ratio increasing from $M=0.3$ to $M=1.5$, the film effectiveness rises monotonically over the downstream area of the cooling holes, suggesting that within the range of blowing ratios tested, increasing the mass flow of coolant will have a positive impact on the film effectiveness. For coolant jets with a mass flux 1.5 times that of the mainstream flow, i.e., $M=1.5$, there is still a significant amount of coolant remaining close to the surface at the downstream position of $X/D = 15$, revealing the capability of a laid-back, fan-shaped hole to reduce the momentum of the coolant at the outlet and keep the coolant close to the surface, which would otherwise lift off and lose contact with the surface if ejected from a cylindrical hole.

Comparing Figure 10 and Figure 11, the effect of a higher density coolant can be shown in a qualitative manner. Coolant is subjected to higher gravitational forces per specific volume with an increased the density, thus being able to stay closer to the surface and have a wider lateral spread, creating a wider and larger area with high effectiveness. This could be confirmed by the increased area with $\eta > 0.5$ in Figure 11 for each blowing ratio. In general, the effect of blowing ratio and density ratio on film cooling effectiveness for laid-back, fan-shaped holes from previous investigations, can be observed in this study.

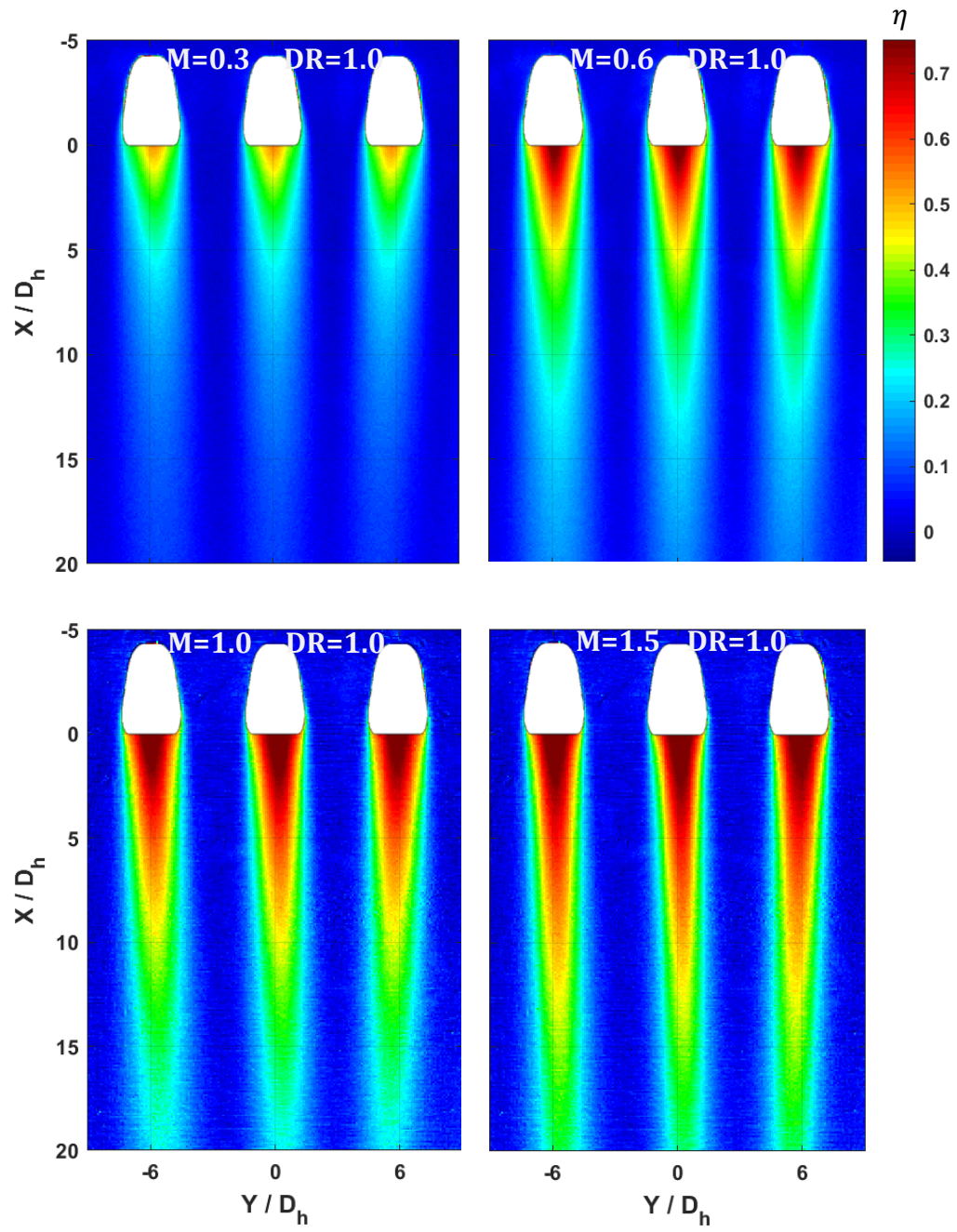


Figure 10 Detailed film cooling effectiveness distributions for fan-shaped holes with cylindrical inlet at $DR=1$.

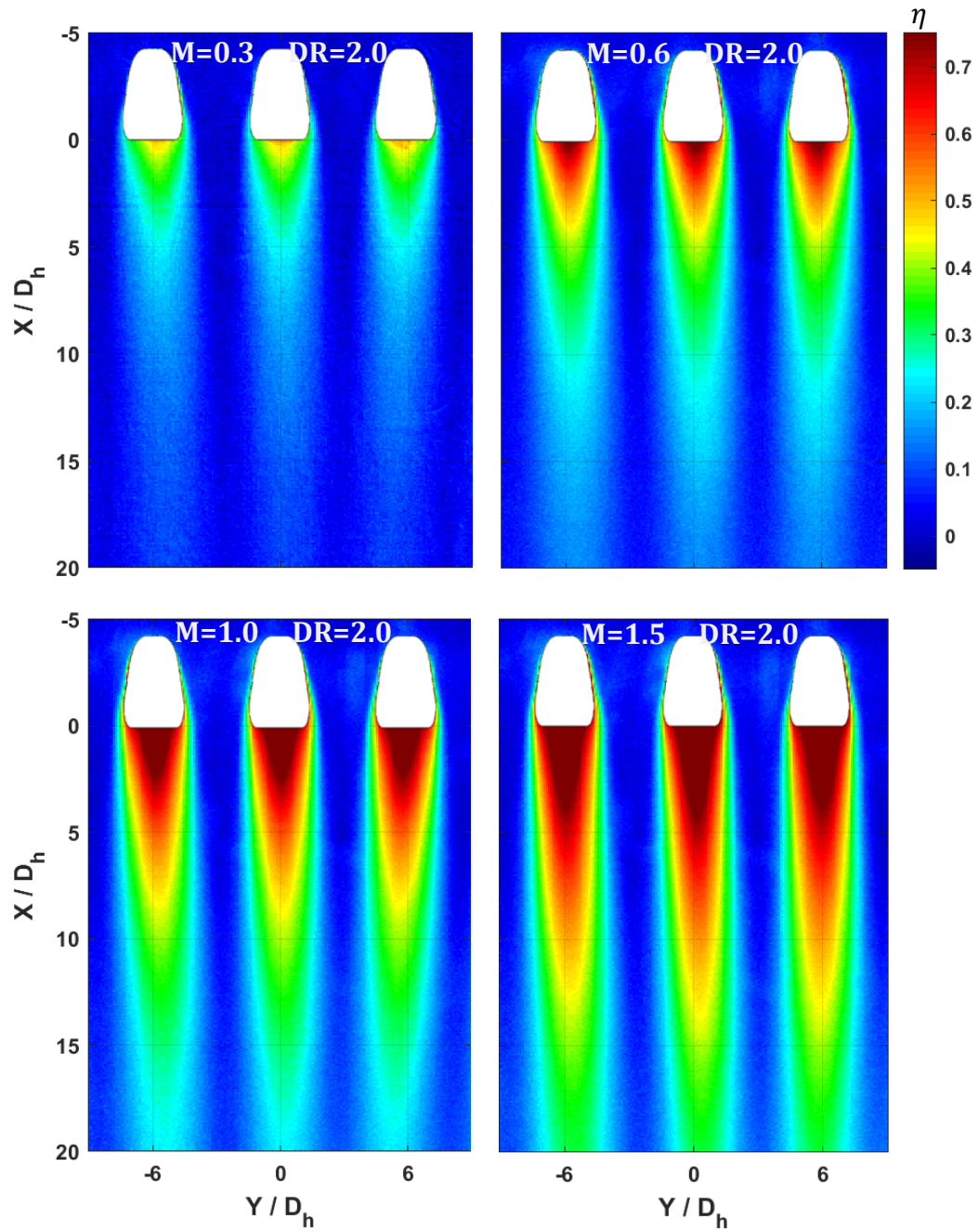


Figure 11 Detailed film cooling effectiveness distributions for fan-shaped holes with cylindrical inlet at $DR=2$.

Fan-shaped holes with the 2:1 aspect ratio inlet

For the results of fan-shaped holes with the 2:1 aspect ratio inlet, the detailed film cooling effectiveness distributions for DR=1 and DR=2 over all blowing ratios are plotted in Figure 12 and Figure 13, respectively.

Similar trends of blowing ratio and density ratios reoccur in Figure 12 and Figure 13, indicating the effect from the laid-back, fan-shaped outlet geometry is not diminished with the 2:1 inlet. The area with high film effectiveness is increased for all the cases for holes with the 2:1 inlet. For cases with the same density ratio, holes with the 2:1 inlet can provide a wider lateral spread and a longer trace of high effectiveness compared with the holes with a cylindrical inlet. For a typical case of DR=1, M=1.5, the regions with $\eta > 0.5$ can be maintained approximately from $0 < X/D_h < 13$ for holes with a cylindrical inlet, while for holes with the 2:1 inlet, this distance can be maintained over $X/D_h \geq 17$. This suggests although the two geometries are of the same outlet cross sectional area, the holes with the 2:1 inlet can keep a higher portion of the ejected coolant in contact with the surface.

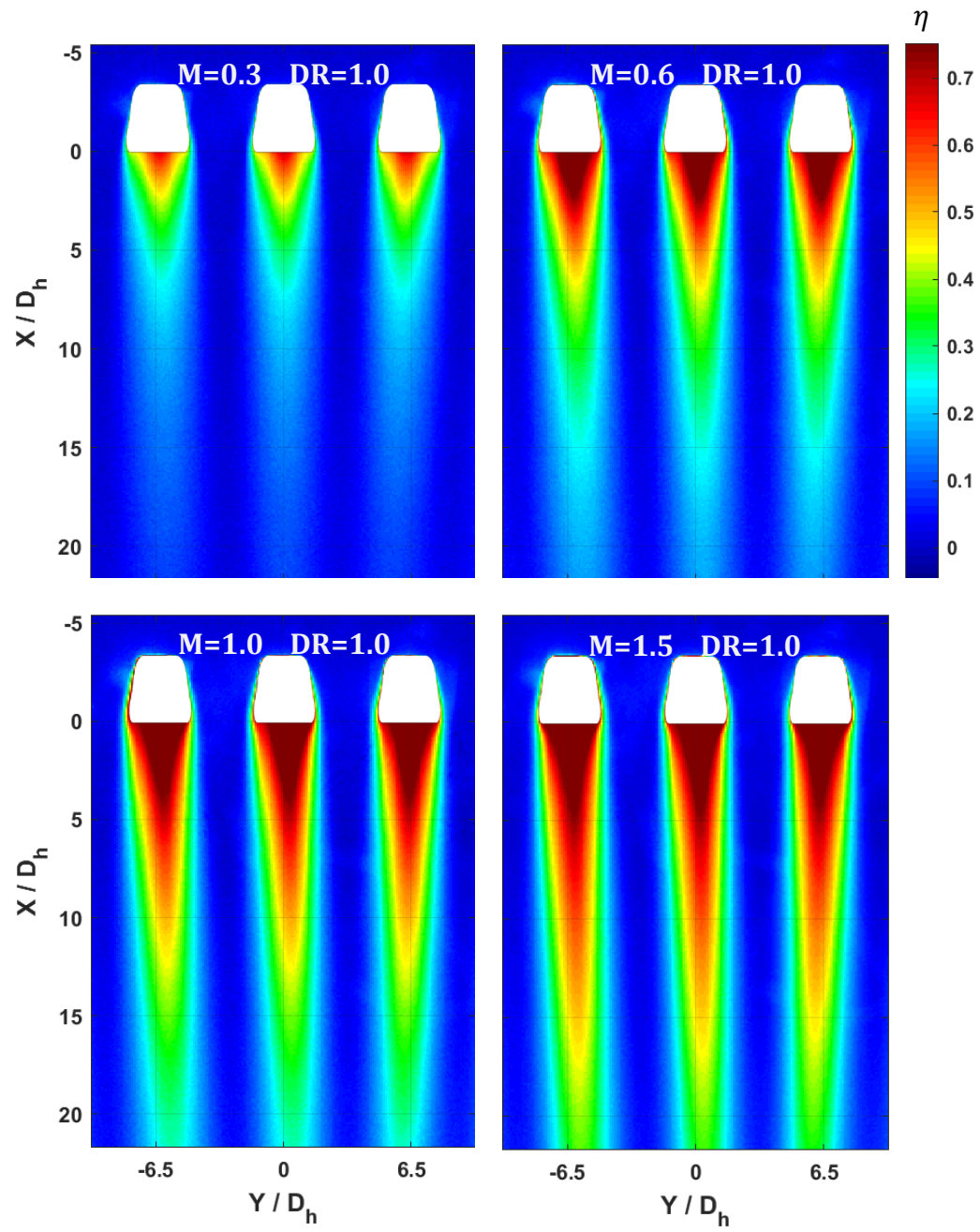


Figure 12 Detailed film cooling effectiveness distributions for fan-shaped holes with the 2:1 aspect ratio inlet at $DR=1.0$.

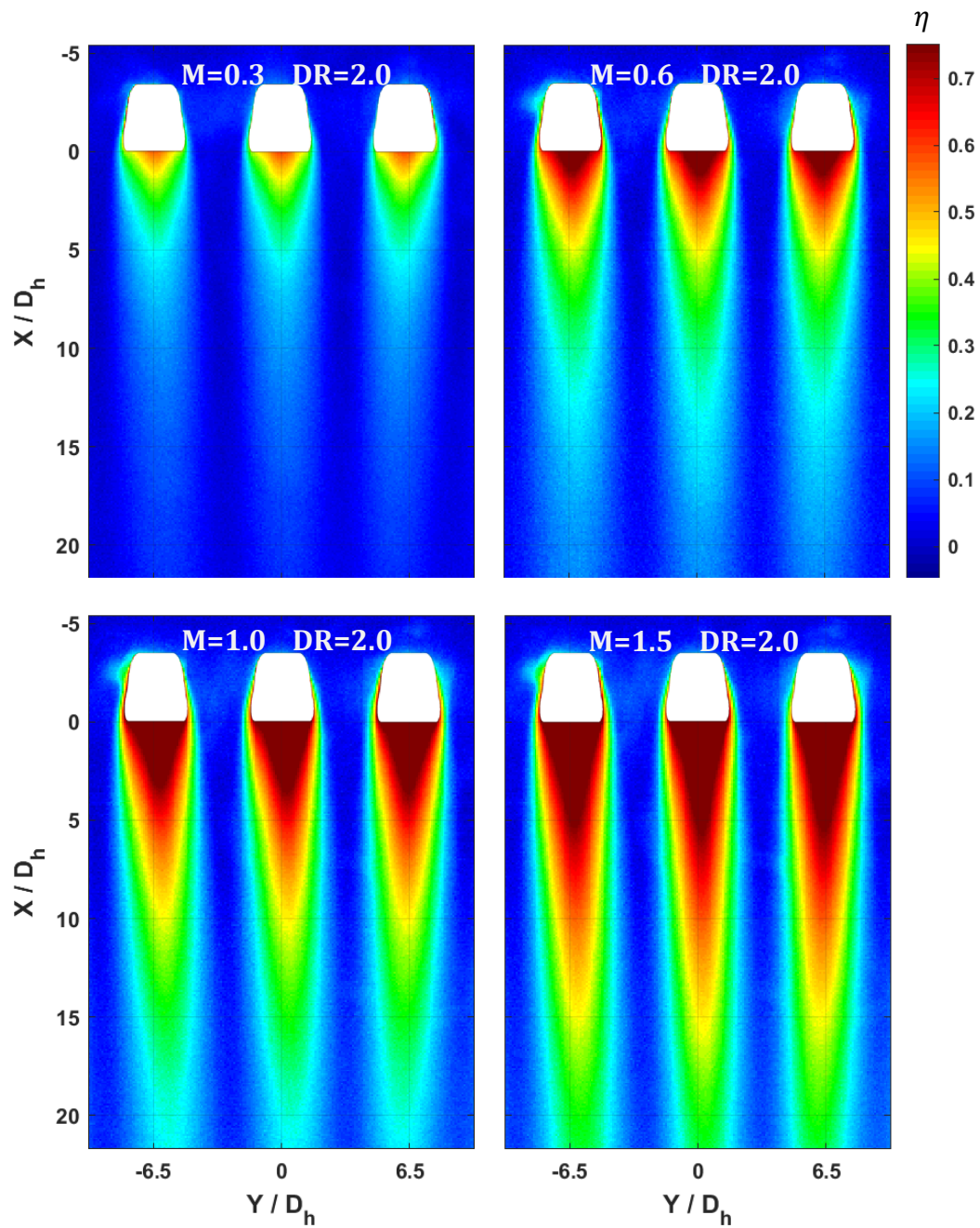


Figure 13 Detailed film cooling effectiveness distributions for fan-shaped holes with the 2:1 aspect ratio inlet at DR=2.

Fan-shaped holes with the 4:1 aspect ratio inlet

For the results of fan-shaped holes with the 4:1 aspect ratio inlet, the detailed film cooling effectiveness distributions are plotted in Figure 14 and Figure 15.

Comparing the 4:1 inlet and the other two inlet geometries, one specific problem for the holes with the 4:1 inlet is that the coolant cannot fully cover the width of the outlet at high blowing ratios of 1 and 1.5 and the coolant plume is biased towards one side of the hole, especially for $DR=1$, when the velocity of the coolant is the highest. This also leads to a narrower trace of coolant over the surface downstream, suggesting a smaller area protected by the coolant. However, at a low blowing ratio of 0.3 and 0.6, the 4:1 hole has better coolant coverage than the other geometries, suggesting this geometry may have problems with high momentum coolant but is better suited for relatively low momentum flows.

Qualitatively comparing the detailed effectiveness distributions of the holes with 4:1, 2:1 and cylindrical inlet, the following phenomena can be observed:

For each of the inlet configurations, the general trends from previous studies of η for laid-back, fan-shaped holes with varying density and blowing are observed. The injected coolant flow can remain attached to the surface for all the cases investigated, with M as high as 1.5. Within the range of blowing ratios investigated, η grows monotonically with M increasing, suggesting higher coolant momentum always has a positive impact on cooling for these geometries. Comparing the results of $DR = 1$ and $DR = 2$, the higher density coolant will lead to better lateral coverage for all geometries, which is expected from the results listed in open literature. From the detailed

distributions, the 2:1 aspect ratio inlet appears to have the greatest potential of increasing the performance of the fan-shaped outlet over a variety of flow conditions, while the 4:1 geometry seems suited for low momentum coolant, but it is not suited for applications with high momentum coolant. In the next section, the comparison and analysis of laterally and area averaged effectiveness will qualitatively help support the qualitative observations obtained from the detailed distribution plots.

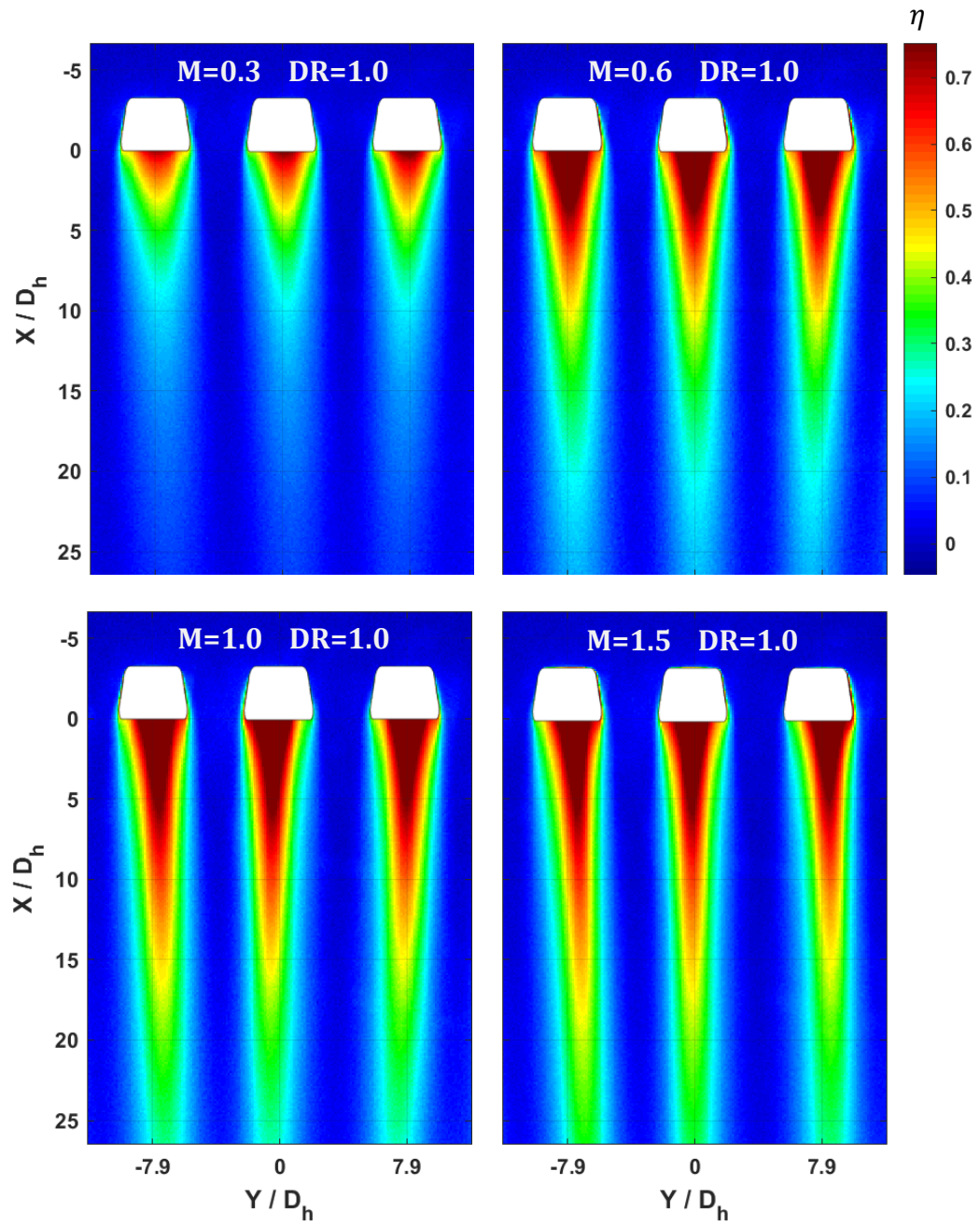


Figure 14 Detailed film cooling effectiveness distributions for fan-shaped holes with the 4:1 aspect ratio inlet at $DR=1$.

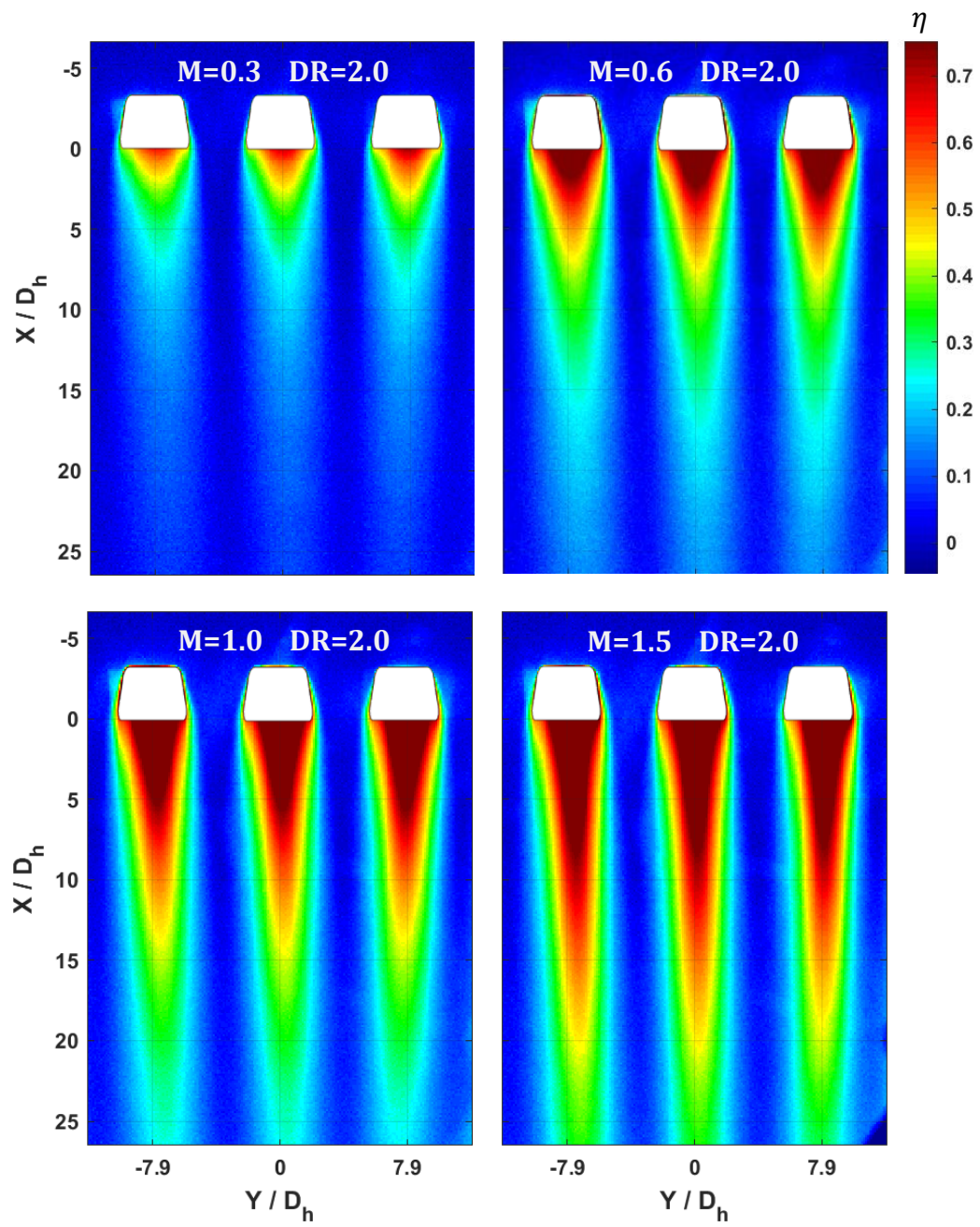


Figure 15 Detailed film cooling effectiveness distributions for fan-shaped holes with the 4:1 aspect ratio inlet at $DR=2.0$.

Performance Comparison over the Range of Flow Conditions and Geometries

Blowing Ratio Effect

For the effect of blowing ratio, Figure 16 shows the laterally averaged film cooling effectiveness, η_{lat} , across the width of the area of interest. From the figure, it can be deduced that for all the geometries investigated, the blowing ratio has a net positive impact on η_{lat} within the range of blowing ratio studied, with the 4:1 inlet using DR=1 coolant as the only exception. It can also be noted as blowing ratio increases over 1.0, the benefit of increased mass flux reduces; the effectiveness continues to increase but at a slower rate than at lower blowing ratios. At the near-hole region ($X/D_h < 3$), it can be noted that the higher momentum coolant has a smaller positive impact on η_{lat} than the coolant regions further downstream. This may be due to the higher momentum coolant jet being more likely to mix with the mainstream flow, decreasing the amount of coolant remaining close to the surface, thus reducing the lateral spread over the surface and the laterally averaged effectiveness.

In the case of DR=1 coolant, for holes with the 4:1 inlet, M=1.0 and M=1.5 provide the same cooling performance. This suggests the transition point of η_{lat} , with respect to the blowing ratio, for this geometry is around 1.5 while the other two geometries still have the potential to further elevate the effectiveness above M=1.5.

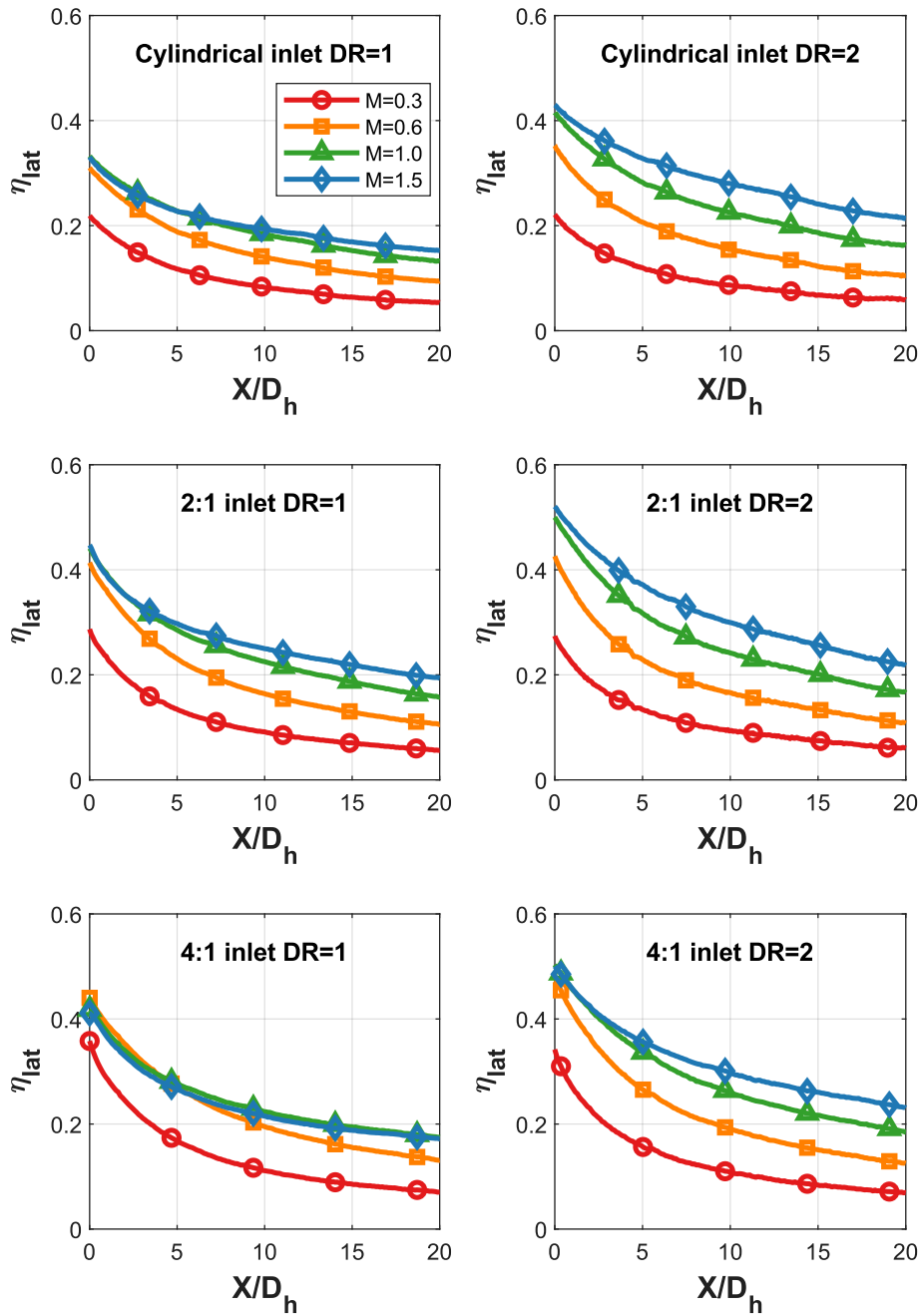


Figure 16 Effect of blowing ratio on the laterally averaged film cooling effectiveness.

Density Ratio Effect

Figure 17, Figure 18 and Figure 19 show the η_{lat} plot with density ratio being the variable. It can be clearly seen in the figures that at lower blowing ratios of 0.3 and 0.6, the density ratio has almost no impact on η_{lat} for all of the geometries, as the jet momentum is so low that it is already kept close to the surface under the influence of high momentum mainstream flow.

At higher blowing ratios, the difference in the varying density ratio becomes more apparent, as the higher density coolant has a positive impact on the film cooling effectiveness. As the blowing ratio increases, the disparity of velocity between coolant jets with different densities become larger and will affect the interaction with the mainstream flow. Higher density coolant itself also tends to stay closer to the surface, as the gravitational force acting on denser coolant is larger by the same volume, offsetting the negative impact of lift-off effect of a high momentum coolant.

It is also worth noting that the positive impact of the higher density slowly diminishes as the flow continues downstream. For a fixed blowing ratio, the higher density coolant requires reduced volume, which is more easily diluted by the mainstream, thus losing coolant near the surface and lowering the effectiveness.

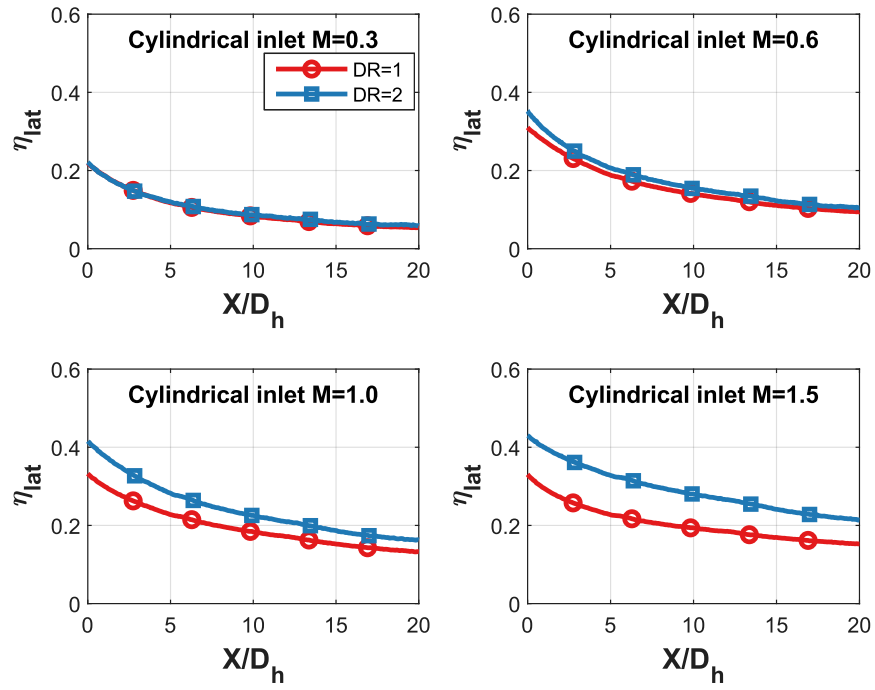


Figure 17 Effect of density ratio on the laterally averaged film cooling effectiveness for holes for shaped holes with a cylindrical inlet.

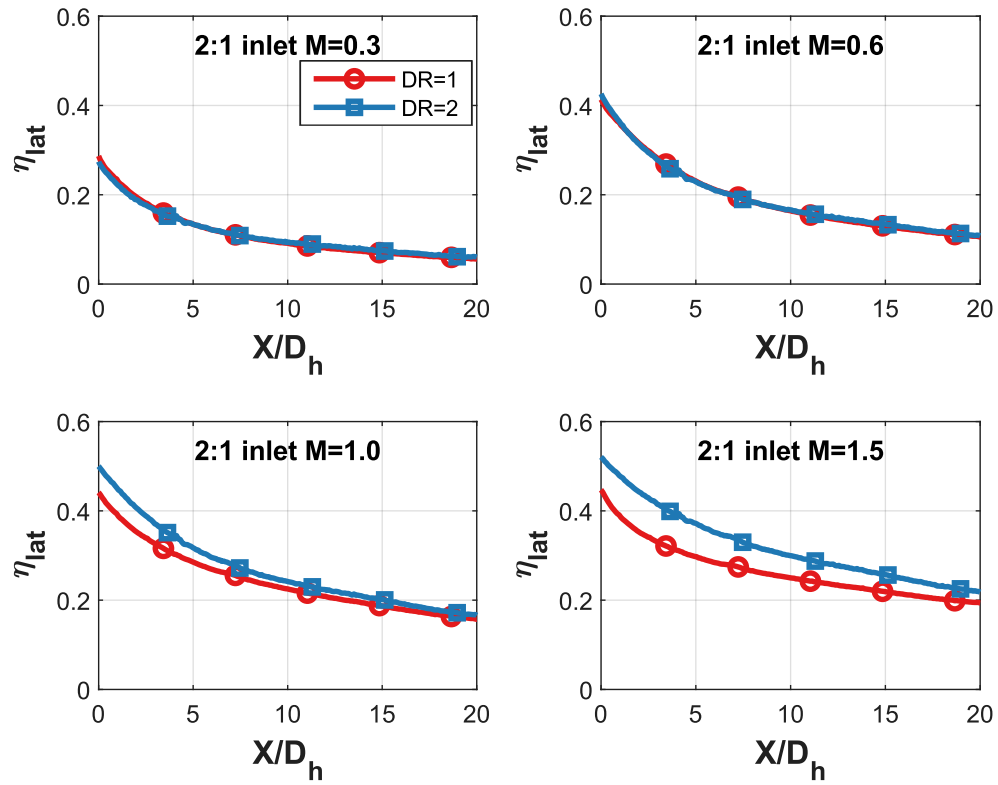


Figure 18 Effect of density ratio on the laterally averaged film cooling effectiveness for shaped holes with the 2:1 inlet.

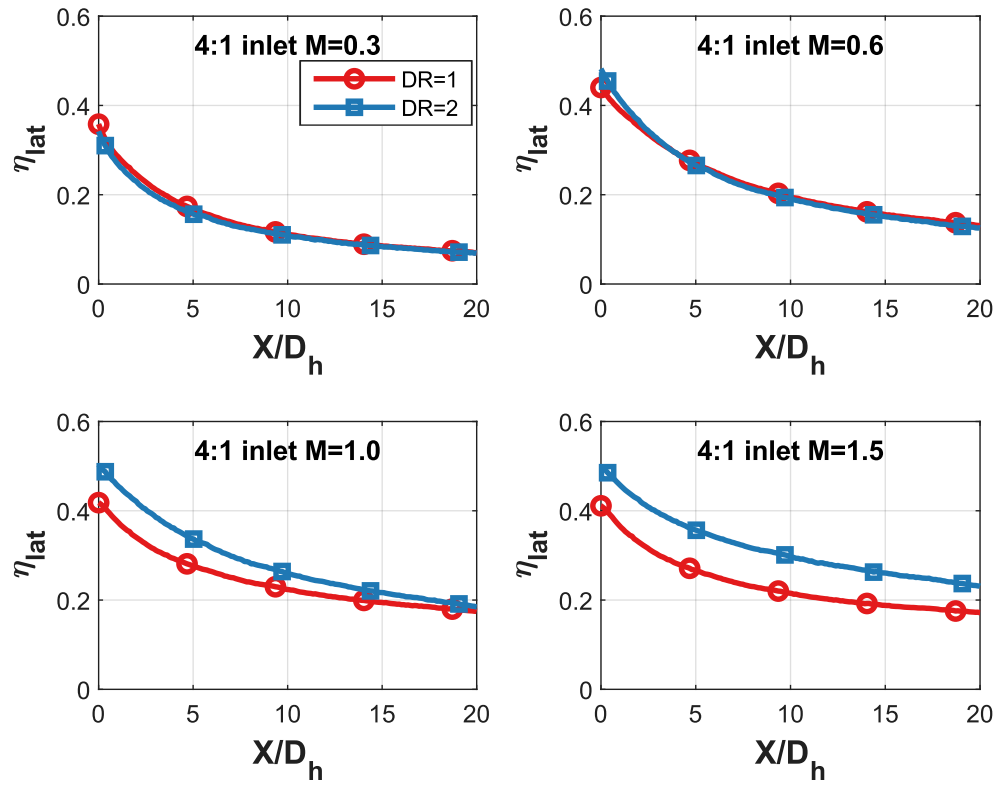


Figure 19 Effect of density ratio on the laterally averaged film cooling effectiveness for shaped holes with the 4:1 inlet.

Inlet Geometry Effect

To better evaluate the performance of the shaped inlets, two predicting correlations are introduced. The first correlation was introduced by S.S. Kutateladze and A. I. Leont'ev [35] and adopted by Goldstein [3] in a comprehensive work on film cooling. It is based on a heat sink model of 2D incompressible flow film cooling, predicting the film effectiveness downstream of a two-dimensional continuous slot. It is defined in equation (10):

$$\eta = \frac{1}{1 + 0.249\xi^{0.8}} \quad (10)$$

Where ξ is a non-dimensional parameter used in the heat sink model, which is defined as follows:

$$\xi = \frac{X}{MS} \quad (11)$$

Where X is the position of a downstream location with respect to the slot, M is the blowing ratio, and S is the width of the slot. Note this correlation is based on the assumption that the coolant and the mainstream flow are of the same density.

The second correlation is the forementioned correlation introduced by Colban et al. [14], which is based on empirical data from various studies conducted on fan-shaped holes. It is defined in equation (12):

$$\eta_{lat} = \frac{1}{\frac{P}{t} + c_1 M^{c_2} \xi^{c_3}} \quad (12)$$

Where constant $c_1 = 0.1721$, $c_2 = -0.2664$, $c_3 = 0.8749$, P is the pitch of the film cooling holes, t is the width of the outlet, M is the blowing ratio, and ξ is the same

non-dimensional parameter in equation (12) and adopted by Colban et al. [14], with the geometric parameters of a shaped cooling hole with a cylindrical inlet taken into consideration, which is defined in equation (13):

$$\xi = \frac{X}{MS} = \frac{4}{\pi} \left(\frac{X}{D} \right) \left(\frac{P}{D} \right) \frac{1}{M \cdot AR} \quad (13)$$

Where S is the equivalent slot width of a discrete film cooling hole cooling scheme, D is the diameter of the cylindrical inlet, and AR is the area ratio of the outlet over the inlet cross sectional area of a shaped hole. Note that this correlation was based on experimental data of $DR=2$ studies.

Figure 20 and Figure 21 depict the performance of different geometries under the same flow conditions, together with the two correlations predicting the performance of a shaped hole with a cylindrical inlet and a slot with the equivalent slot width ejecting the same amount of coolant. Note that in this study, the outlet area, $A_{out} = AR \cdot A_{in}$, and the pitch, P , are the same for all geometries, thus the equivalent slot width, S , are also the same. Although the range of x-axis of each figure varies with X/MS , since M and S remain constant for each flow condition, the figures can still reflect the non-dimensional performance of the film cooling holes. To see the effectiveness plot against physical distance or non-dimensional X/D_h , reference the figures listed in Appendix A.

Comparing the experimental results themselves, for all the flow conditions, holes with shaped inlets in general have better performance over holes with the traditional, cylindrical inlet. At lower blowing ratios of 0.3 and 0.6, holes with the 4:1 inlet slightly outperform those with the 2:1 inlet, especially at the near-hole region. While the 2:1 inlet

geometry provides increased effectiveness for coolant with increased blowing ratios of $M=1.0$ and $M=1.5$. In the cases with $DR=1$ in Figure 20, the 2:1 inlet is observed to have a η_{lat} improvement with increasing coolant momentum, this trend, however, is not as apparent for $DR=2$ in Figure 21. At the elevated density ratio, the effect of inlet geometry is reduced for all blowing ratios. Increasing the blowing ratio increases the effectiveness for all geometries. In regions further downstream, the effectiveness curve of all inlet geometries collapses together.

As the correlation for fan-shaped holes was based solely on $DR=2$ data, the comparison of the experimental data obtained in the current study and the correlations will be restricted for the density ratio of $DR=2$. For all the flow conditions, results of the fan-shaped holes with a cylindrical inlet in this study have a good match with both correlations in downstream regions, suggesting results from the current study are comparable with previous investigations. For the shaped inlets, both shaped inlet geometries contribute to an elevated film cooling effectiveness in near hole regions compared to the cylindrical inlet. The effectiveness is equivalent or higher than the prediction of the correlation for fan-shaped holes, yet it is still lower than the effectiveness calculated from the 2D slot correlation. This implies the flow behavior of the coolant ejected from shaped inlets becomes more akin to the 2D slot flow, probably due to reduced mixing losses from the anti-kidney vortices induced by the shaped inlets, compared with a cylindrical inlet. In regions further downstream, the effectiveness curves collapse together at low blowing ratios, indicating the effect of the inlet on the flow is more restricted in the near hole region.

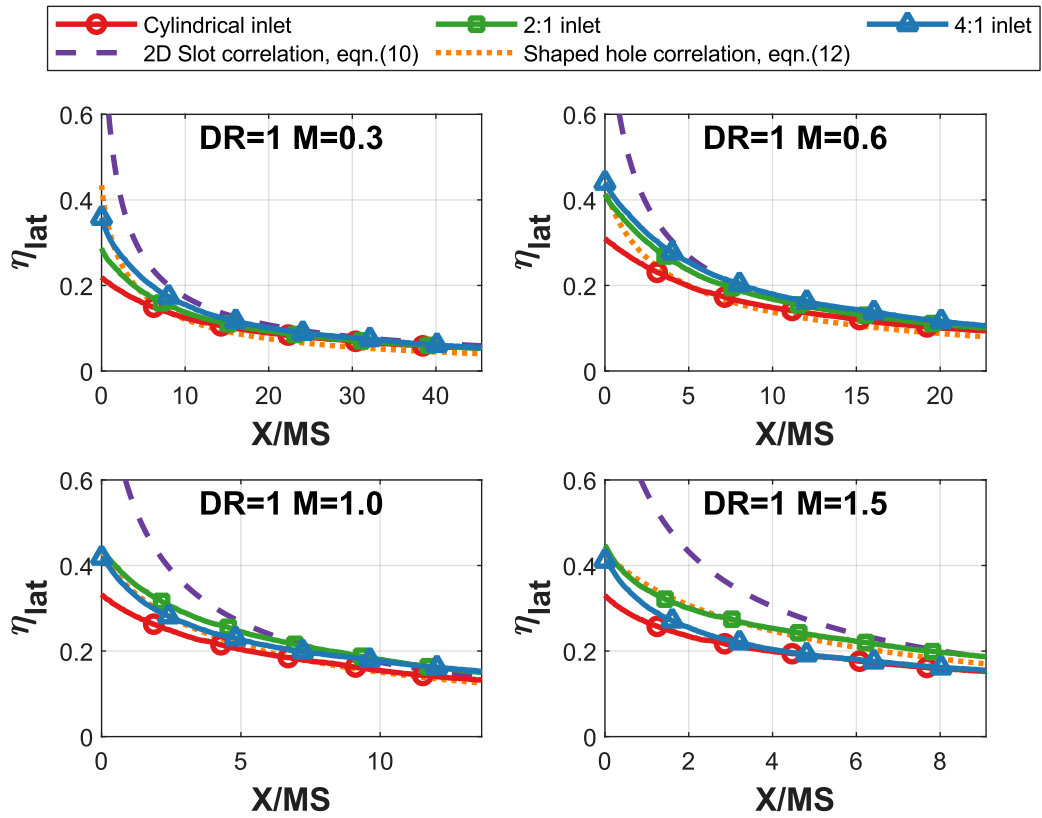


Figure 20 Effect of inlet geometry on the laterally averaged film cooling effectiveness at $DR=1.0$, with predicting correlations as comparison.

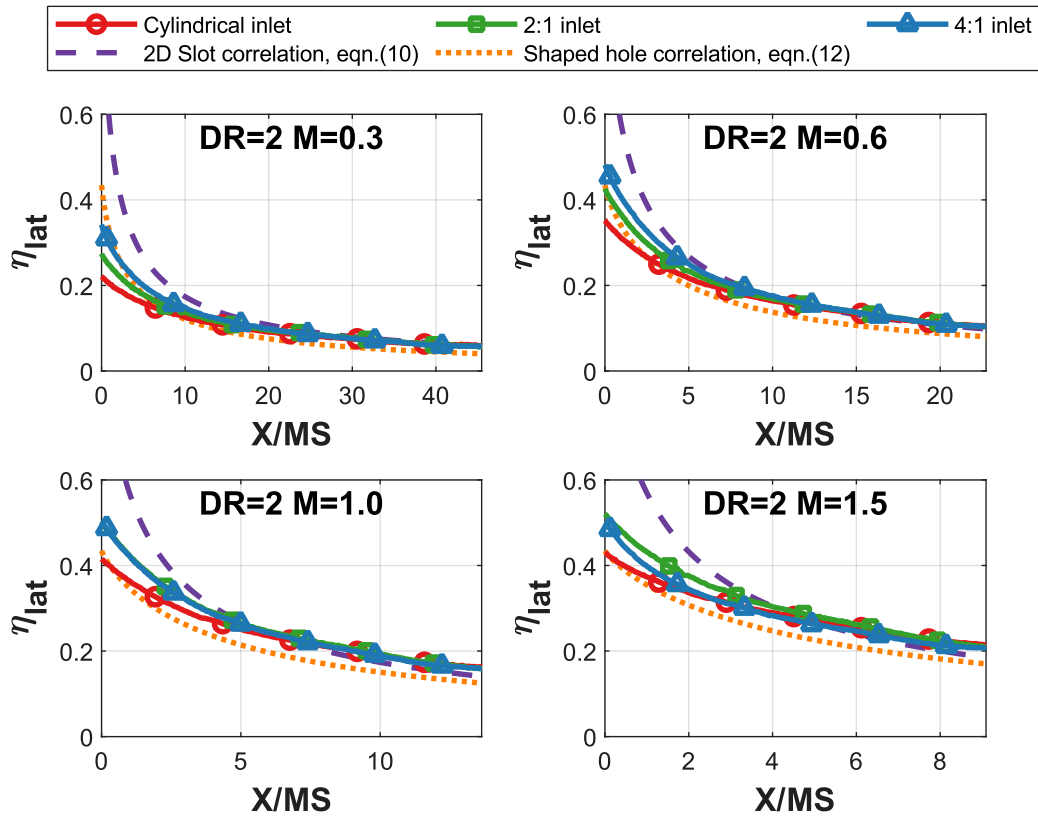


Figure 21 Effect of inlet geometry on the laterally averaged film cooling effectiveness at DR=2.0, with predicting correlations as comparison.

To further assess the performance of the shaped inlets, the momentum flux ratio, I , is introduced and coupled with the area averaged film cooling effectiveness η_{area} to have an overall understanding of all cases studied. Figure 22 clearly shows the advantage of shaped inlets over cylindrical inlets at all flow conditions studied.

The slopes of η_{area} are similar for the same inlet geometry at similar momentum flux ratios, from which it can be inferred that the transitional momentum flux ratio signaling a negative impact from the increased mixing with the mainstream for the 4:1 inlet is at roughly at $I \sim 1$ while the transitional momentum flux ratio for the cylindrical

and the 2:1 inlet are larger, which implies for coolant flows with higher momentum flux ($I > 1$), the 2:1 inlet is more suitable. While for flows with a low momentum flux ($I < 0.5$), the 4:1 inlet has a small advantage over the other two geometries.

For tests of $DR=1$, η_{area} of holes with the 2:1 inlet is can be 20%-25% higher than that for the cylindrical inlet holes, the difference is reduced to approximately 10% when density ratio increases to $DR=2$. For holes with the 4:1 inlet, the advantage at lower momentum flux ratios over cylindrical inlet holes is about the same or slightly higher than the 2:1 inlet, but this quickly drops to only about 5% at $M=1.5$.

By referencing the detailed distributions from Figure 10 to Figure 15, the picture is more clear that the coolant injected from holes with the 2:1 inlet forms wider plumes with higher η covering the area at higher blowing ratios, while coolant from holes with the 4:1 inlet can from higher η regions immediately downstream, but the plumes with higher momentum get narrower further downstream and cannot provide full coverage across the width, suggesting more coolant mixing into the mainstream and the coverage of the film is reduced. All these can support the conclusions drawn from the $X/D_h - \eta_{lat}$ plots and the $I - \eta_{area}$ plot.

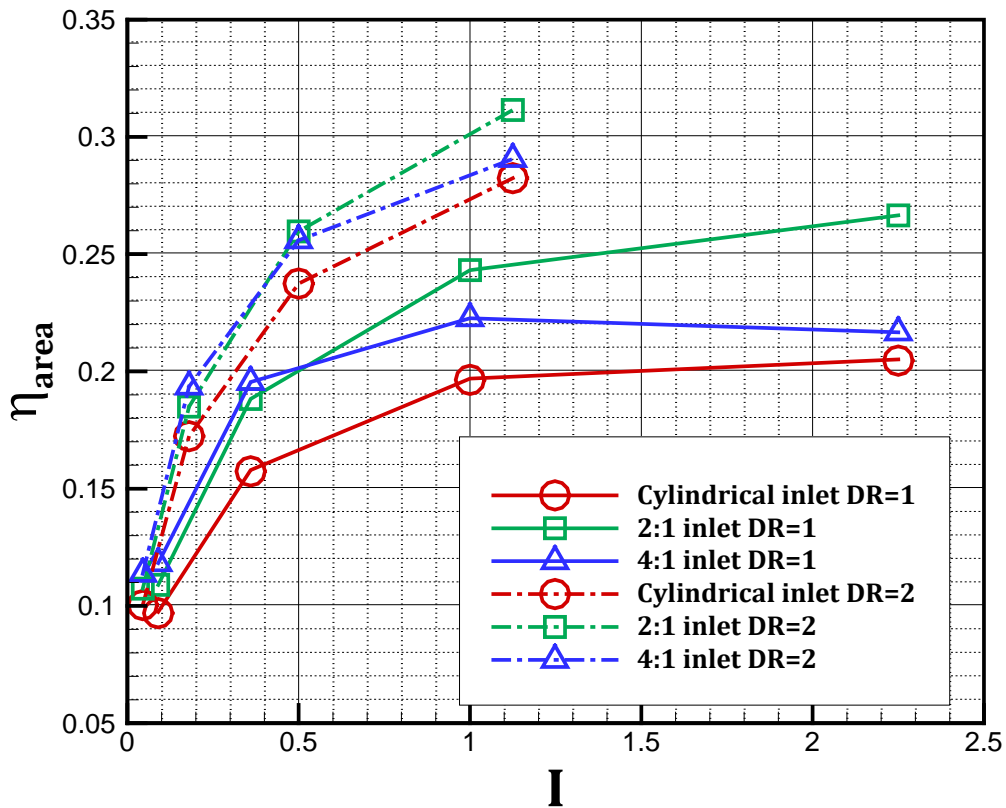


Figure 22 Area averaged effectiveness of the same area of interest in terms of momentum flux ratio.

The driving mechanics behind these phenomena may still be related to the counter-rotating vortices formed by the interaction between the jet and the crossflow. From the work of Haven and Kurosaka [24], a wider hole resulting from a larger aspect ratio inlet will introduce a stronger anti-kidney vortex pair to counter the tendency of the jet lifting up, thus increasing the film cooling effectiveness. When coupled with the laid-back, fan-shaped outlet which also promotes such flow behavior, film cooling performance can be further increased as is shown by the experiment results. However, the reason behind higher aspect ratio 4:1 inlet having reduced performance compared to

the medium aspect ratio of 2:1 at higher blowing ratios is not exactly known and should be further investigated. However, this infers there is an optimum operating blowing ratio for a specific inlet geometry, which does not always increase with the aspect ratio of the inlet.

When designing gas turbines, the results from this study could serve as a useful insight when it comes to optimizing the design of the film cooling holes geometry and layout. Depending on the position of the holes, mainstream and coolant properties, and the area downstream that requires film protection, a proper inlet geometry design could further contribute to a more efficient and more effective external cooling scheme. For example, from the results of this study, holes with the 2:1 inlet should be used regions and with high momentum flux ratios with larger area downstream to be protected, and holes with the 4:1 inlet can be used to save coolant in regions that only requires protection immediate downstream of the holes.

Film Cooling Effectiveness Uncertainty Analysis

The uncertainty analysis in this study is based upon the work of Natsui et al. [36] to quantify the uncertainty of PSP experiments. This work also follows the principles listed in PTC 19.1 [37] regarding the uncertainty of the results of single-sample experiments, as well as the principles put forward by Kline and McClintock [38] On a pixel-by-pixel basis, the standard deviation of light intensity is calculated for a certain set of black, reference, air, or coolant-air mixture images. The standard deviation is regarded as the uncertainty of intensity measurement $U_{I,ref/air/mix}$. It is then propagated into the calculation of intensity ratio uncertainty U_{IR} , pressure ratio uncertainty U_{PR} and ultimately, the uncertainty of film cooling effectiveness U_{η} . The uncertainty from both PR_{air} and PR_{mix} are taken into consideration. In general, the regions with high emission intensity tends to have low uncertainty, and regions with low emission intensity have high uncertainty, which implies the measurement in regions with high film cooling effectiveness is of low uncertainty.

Figure 23 provide a typical detailed distribution of the absolute and relative uncertainty (2:1 inlet, DR=1, M=1.5). In Figure 24, the film cooling effectiveness, the absolute uncertainty, and the relative uncertainty along the centerline ($Y/D_h = 0$) of the flat plate are shown. In regions with $\eta \approx 0.7$, the uncertainty is about 4.5%. While in regions with $\eta \approx 0.4$, the uncertainty increases to about 17%. For DR=2 tests, the density ratio, DR, in equation (8) will act as multiplying constants when calculating the uncertainty, the uncertainty in regions with a similar effectiveness will be different than

that this DR=1 case. Generally, the uncertainty increases with increasing density ratio in regions with a low effectiveness. Note that all the uncertainties calculated above is for a single experiment.

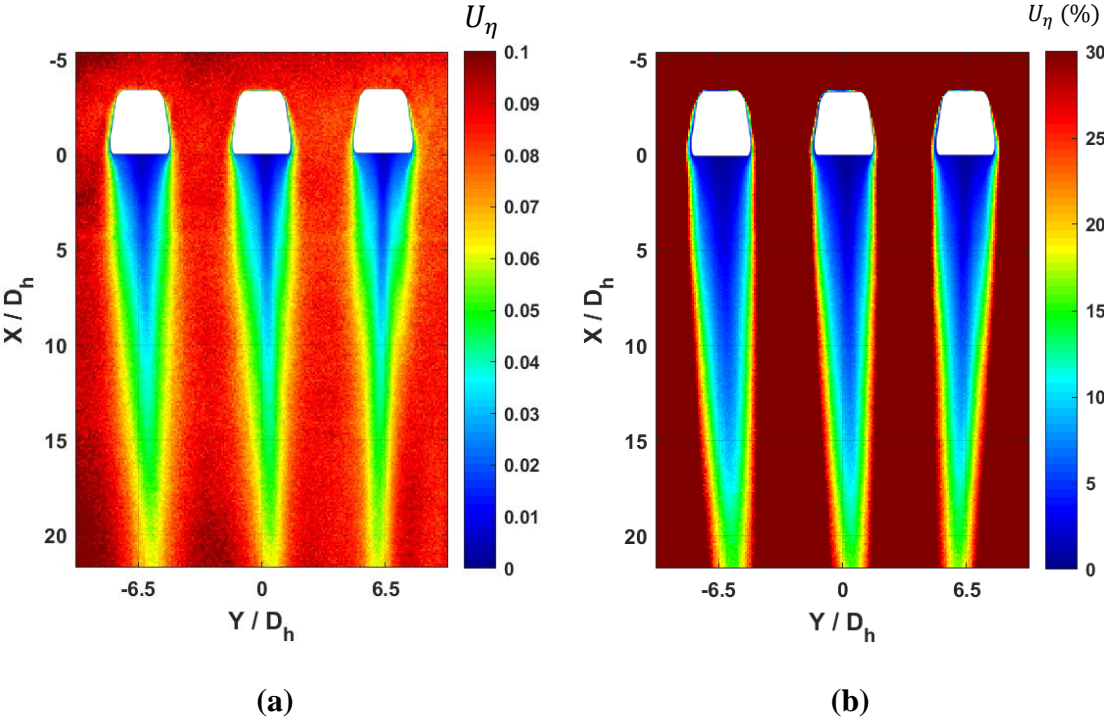


Figure 23 Uncertainty of the film cooling effectiveness for 2:1 inlet, DR=1, M=1.5. (a)absolute uncertainty (b)relative uncertainty.

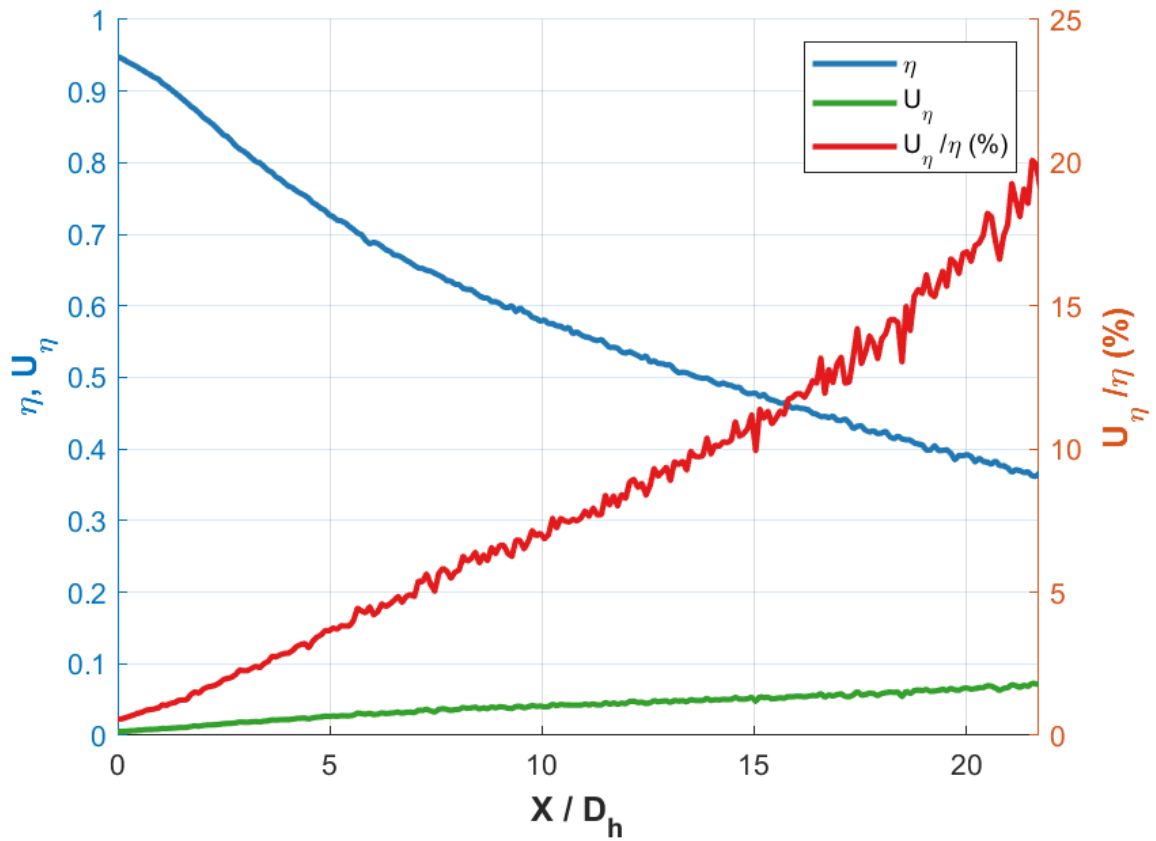


Figure 24 Film cooling effectiveness, the absolute and relative uncertainty along the centerline of the test section for DR=1, M=1.5 test of holes with the 2:1 inlet.

Effect of Inlet Geometry on the Discharge Coefficient

In addition to the film cooling effectiveness measurements, the effect of the shaped inlet geometries on the discharge coefficient, C_d , was also measured and presented. According to Han et al. [5], the discharge coefficient is vital to the sizing of film cooling holes during the design process, to determine the amount of coolant necessary to produce the desired film effectiveness. It is calculated in the following equation, according to Burd and Simon [39]:

$$C_d = \frac{\dot{m}_c}{A\sqrt{2\rho_c(P_{c,t} - P_{\infty,s})}} \quad (15)$$

Where \dot{m}_c is the mass flow rate of the coolant, corresponding to the blowing ratios during the film cooling effectiveness measurements; A is the total inlet cross-sectional area of all the film cooling holes, ρ_c is the density of the coolant; $P_{c,t}$ is the total pressure of the coolant inside the plenum, which is measured by a pressure tap in the plenum, and P_{∞} is the static pressure of the mainstream flow, which is obtained by a Pitot-static tube in the mainstream. All the pressures are measured with a digital manometer with an accuracy of 0.001kPa.

The discharge coefficients of all inlet geometries under all flow conditions investigated during this study are plotted against momentum flux ratio, I , in Figure 25, and pressure ratio, $P_{c,t}/P_{\infty,s}$, in Figure 26.

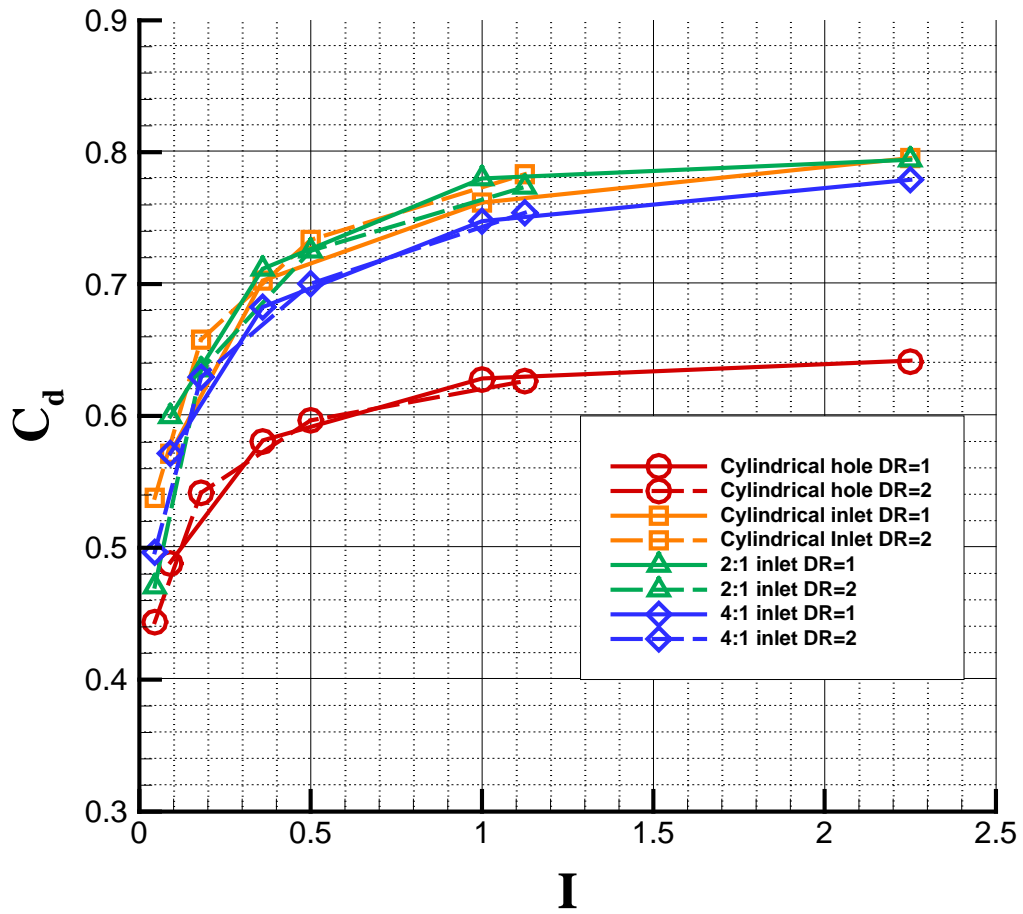


Figure 25 The variation of discharge coefficient with momentum flux ratio.

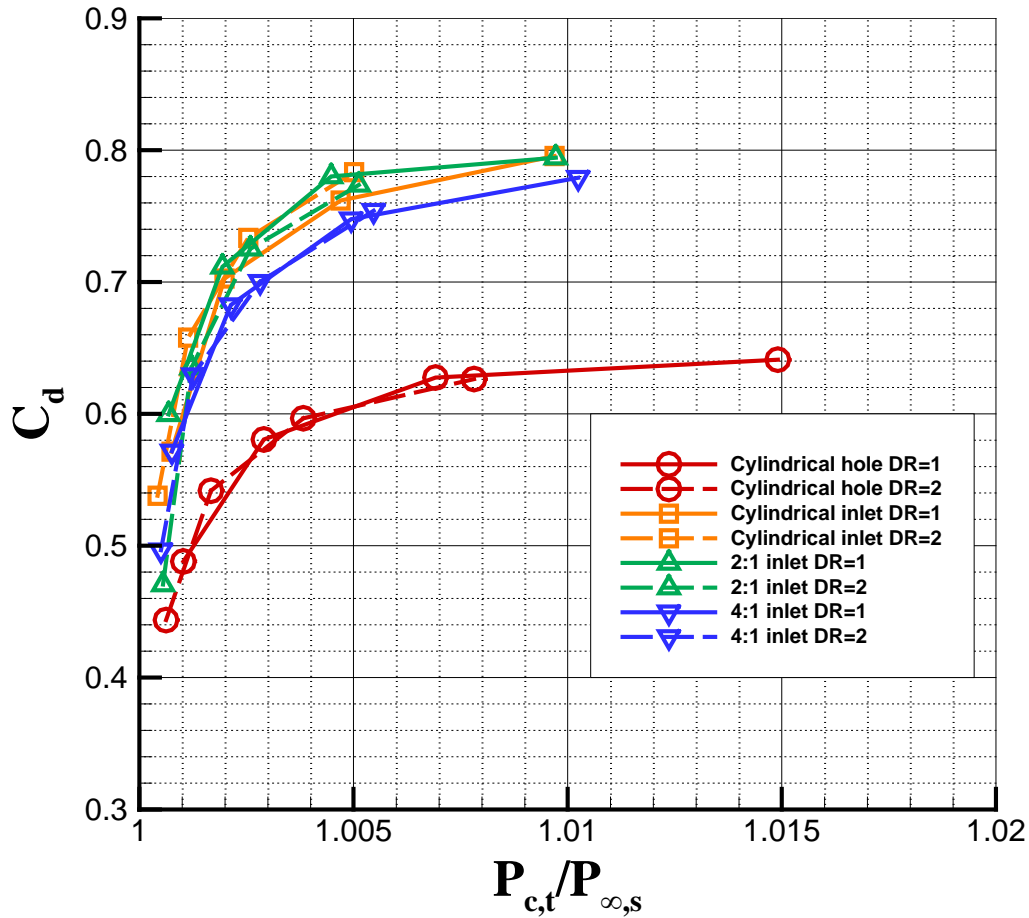


Figure 26 The variation of discharge coefficient with coolant-mainstream pressure ratio.

Figure 25 indicates that, at the same momentum flux ratio, the 2:1 inlet has similar performance, in terms of discharge coefficient, under most conditions, except at a very low momentum flux ratio, $I = 0.045$ (equivalent to $DR = 2, M = 0.3$), the discharge coefficient of the 2:1 inlet is 0.06 lower than the cylindrical inlet. This may also be due to increased measurement uncertainty for a coolant flow with low mass flow rates. For the 4:1 inlet, the discharge coefficient is constantly 0.02-0.04 lower than the

cylindrical inlet under all the flow conditions, suggesting the flow resistance of the 4:1 inlet is generally larger. All the fan-shaped cooling holes with different types of inlets show an improvement in discharge coefficient over the cylindrical hole, which can be confirmed from previous studies by Gritsch et al. [40]. It can also be observed that higher density ratio coolant has a smaller discharge coefficient for the same blowing ratio, as the volumetric flow rate is reduced. The discharge coefficients of different flow conditions for the same inlet geometry fall on the same curve, suggesting that the discharge coefficient characteristics are consistent for a specific geometry regardless of coolant density.

Figure 26 implies that the 2:1 inlet basically follows the same trend as the cylindrical inlet, suggesting that the excess pressure in the plenum required for the 2:1 inlet to achieve about the same discharge coefficient as the cylindrical inlet is equivalent, again, with the case of $I = 0.045$ (equivalent to $DR = 2$, $M = 0.3$) as an exception. For the 4:1 inlet, it shows that the pressure ratio is larger than the cylindrical inlet under all flow conditions. When the required discharge coefficient is larger than 0.75, the required overpressure for the 4:1 inlet will dramatically increase, for the cylindrical and 2:1 inlet, this threshold is about 0.77-0.78. This confirms the fact that the resistance along the flow path is slightly larger for the 4:1 inlet.

To conclude, the 2:1 inlet has about the same discharge coefficients as the cylindrical inlet in a laid-back, fan-shaped cooling hole, while the 4:1 inlet requires a larger overpressure to achieve the same outcome, suggesting a larger flow resistance.

CHAPTER V

CONCLUSIONS AND FUTURE RECOMMENDATIONS

Systematic efforts were carried out to evaluate the effect of inlet geometry on the film cooling effectiveness over a flat plate. The film effectiveness was measured using a pressure sensitive paint (PSP) technique. The blowing ratio ranged from $M = 0.3 - 1.5$ and density ratios of $DR=1$ and 2 were tested. The mainstream turbulence intensity $Tu\%$ was maintained at 6% . The performances of inlet geometries including traditional cylindrical shape, as well as $2:1$ and $4:1$ aspect ratio “racetrack” shapes were coupled with a common laid-back, fan-shaped outlet geometry. Discharge coefficients were also measured under the forementioned flow conditions.

From the results of this study, the following conclusions can be drawn:

- Shaped inlets with aspect ratios larger than $1:1$ can improve performance of laid back, fan-shaped film cooling holes in all flow conditions tested. The shaped inlets make the flow behavior more akin to flow ejected from a continuous slot.
- For the $2:1$ inlet using $DR=1$ coolant, the improvement of the area averaged effectiveness can reach $20-25\%$, and for $DR=2$ coolant this advantage is reduced to 10% .
- For the $4:1$ inlet the improvement in effectiveness is about the same or slightly higher than the $2:1$ inlet when $I < 0.5$, but this advantage diminishes to 5% with I is increased to 2.25 .

- The shaped inlets generally follow the trend in which cylindrical inlet behaves under various blowing ratios and density ratios, but for different shaped inlets, the performance transition point varies with the momentum flux ratio of the coolant.
- The 2:1 inlet is more suited for improving the average film cooling effectiveness over a larger downstream area with coolant of higher momentum flux ratios.
- Compared with the cylindrical and the 4:1 inlet, the 2:1 inlet can provide a more uniform and widespread film coverage downstream. At higher momentum flux ratios ($I > 1$), the coolant injected from holes with the 4:1 inlet cannot fully cover the width of the hole.
- The 4:1 inlet is more suited for improving the film cooling effectiveness in areas closer to the holes ($X/D_h < 5$).
- The 2:1 inlet has about the same discharge coefficient characteristics as the cylindrical inlet, while the 4:1 inlet has a 0.02-0.04 lower discharge coefficient than the cylindrical inlet under the same flow condition.

Based on the findings of this study, it can be deduced that the “racetrack” shaped inlet geometries in a shaped hole design are superior to traditional cylindrical inlets under various flow conditions. For further evaluation and possible industrial application of the shaped inlets, here are some of the recommendations:

- As the PSP technique can only measure the film cooling effectiveness, heat transfer experiments should be carried out to evaluate the effect of inlet geometry on the heat transfer coefficient.

- The range of flow conditions in this investigation is not large enough to capture the performance transition points of all inlet geometries. Future investigations should include a larger range of blowing ratios and density ratios.
- Future investigations should include an analysis of the flow field using techniques such as PIV to obtain the characteristics of the kidney and anti-kidney CVPs downstream of fan shaped holes with shaped inlets, revealing the underlying mechanism for the increased performance from the shaped inlets.
- Computational methods may be of great help in determining what inlet geometry best suits a certain combination of flow condition and the geometry of downstream area.
- Other characteristic of the shaped inlets, such as manufacturing cost and discharge coefficient should also be investigated in the future to provide a full picture on the feasibility of actual industrial application.
- If the manufacturing cost and turbine structural strength is not taken into consideration, the 2:1 inlet is an overall better alternative to the existing cylindrical inlet for laid-back, fan-shaped cooling holes in terms of performance.

REFERENCES

- [1] Yuri, M., Masada, J., Tsukagoshi, K., Ito, E., and Hada, S., 2013, "Development of 1600 C-class high-efficiency gas turbine for power generation applying J-Type technology," *Mitsubishi Heavy Industries Technical Review*, 50(3), pp. 1-10.
- [2] Han, J.-C., and Rallabandi, A. P., 2010, "TURBINE BLADE FILM COOLING USING PSP TECHNIQUE," *Frontiers in Heat and Mass Transfer*, 1(1).
- [3] Goldstein, R. J., 1971, "Film cooling," *Advances in heat transfer*, Elsevier, pp. 321-379.
- [4] Bogard, D. G., and Thole, K. A., 2006, "Gas turbine film cooling," *Journal of propulsion and power*, 22(2), pp. 249-270.
- [5] Han, J.-C., Dutta, S., and Ekkad, S., 2013, *Gas Turbine Heat Transfer Technology*, CRC Press, pp. 226-227.
- [6] Goldstein, R. J., Eckert, E. R. G., and Burggraf, F., 1974, "Effects of hole geometry and density on three-dimensional film cooling," *International Journal of Heat and Mass Transfer*, 17(5), pp. 595-607.
- [7] Pedersen, D. R., Eckert, E. R. G., and Goldstein, R. J., 1977, "Film Cooling With Large Density Differences Between the Mainstream and the Secondary Fluid Measured by the Heat-Mass Transfer Analogy," *Journal of Heat Transfer*, 99(4), pp. 620-627.
- [8] Johnson, B., Tian, W., Zhang, K., and Hu, H., 2014, "An experimental study of density ratio effects on the film cooling injection from discrete holes by using PIV and PSP techniques," *International Journal of Heat and Mass Transfer*, 76, pp. 337-349.
- [9] Bons, J. P., Macarthur, C. D., and Rivir, R. B., 1996, "The Effect of High Free-Stream Turbulence on Film Cooling Effectiveness," *Journal of Turbomachinery*, 118(4), pp. 814-825.
- [10] Schroeder, R. P., and Thole, K. A., 2016, "Effect of High Freestream Turbulence on Flowfields of Shaped Film Cooling Holes," *Journal of Turbomachinery*, 138(9).
- [11] Gritsch, M., Schulz, A., and Wittig, S., 1998, "Adiabatic Wall Effectiveness Measurements of Film-Cooling Holes With Expanded Exits," *Journal of Turbomachinery*, 120(3), pp. 549-556.
- [12] Wright, L. M., McClain, S. T., and Clemenson, M. D., 2011, "Effect of Density Ratio on Flat Plate Film Cooling With Shaped Holes Using PSP," 133(4), p. 041011.
- [13] Bunker, R. S., 2005, "A Review of Shaped Hole Turbine Film-Cooling Technology," *Journal of Heat Transfer*, 127(4), pp. 441-453.
- [14] Colban, W. F., Thole, K. A., and Bogard, D., 2011, "A Film-Cooling Correlation for Shaped Holes on a Flat-Plate Surface," *Journal of Turbomachinery*, 133(1), p. 011002.
- [15] Haven, B. A., Yamagata, D. K., Kurosaka, M., Yamawaki, S., and Maya, T., 1997, "Anti-Kidney Pair of Vortices in Shaped Holes and Their Influence on Film Cooling Effectiveness," *Proc. ASME 1997 International Gas Turbine and Aeroengine Congress and Exhibition*.

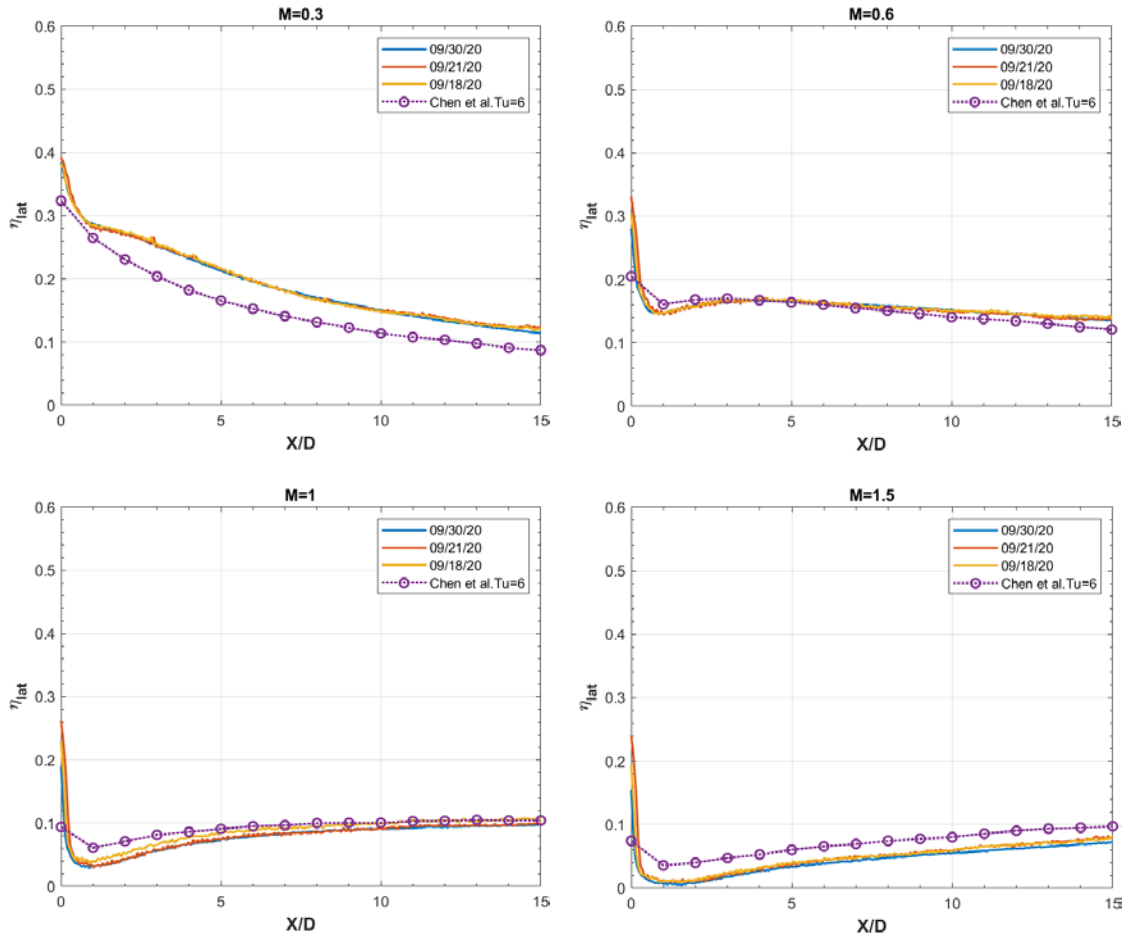
- [16] Lee, K.-D., and Kim, K.-Y., "Shape Optimization of a Laidback Fan-Shaped Film-Cooling Hole to Enhance Cooling Performance," Proc. ASME Turbo Expo 2010: Power for Land, Sea, and Air, pp. 1447-1458.
- [17] Heidmann, J. D., and Ekkad, S., 2008, "A Novel Antivortex Turbine Film-Cooling Hole Concept," 130(3), p. 031020.
- [18] Kusterer, K., Elyas, A., Bohn, D., Sugimoto, T., Tanaka, R., and Kazari, M., "Film Cooling Effectiveness Comparison Between Shaped- and Double Jet Film Cooling Holes in a Row Arrangement," Proc. ASME Turbo Expo 2010: Power for Land, Sea, and Air, pp. 1503-1515.
- [19] Kusterer, K., Elyas, A., Bohn, D., Sugimoto, T., Tanaka, R., and Kazari, M., "The NEKOMIMI Cooling Technology: Cooling Holes With Ears for High-Efficient Film Cooling," Proc. ASME 2011 Turbo Expo: Turbine Technical Conference and Exposition, pp. 303-313.
- [20] Funazaki, K.-I., Nakata, R., Kawabata, H., Tagawa, H., and Horiuchi, Y., "Improvement of Flat-Plate Film Cooling Performance by Double Flow Control Devices: Part I — Investigations on Capability of a Base-Type Device," American Society of Mechanical Engineers.
- [21] Kawabata, H., Funazaki, K.-i., Nakata, R., Tagawa, H., and Horiuchi, Y., "Improvement of Flat-Plate Film Cooling Performance by Double Flow Control Devices: Part II—Optimization of Device Shape and Arrangement by Experiment-and CFD-Based Taguchi Method," Proc. Turbo Expo: Power for Land, Sea, and Air, American Society of Mechanical Engineers.
- [22] Lu, Y., Dhungel, A., Ekkad, S. V., and Bunker, R. S., 2008, "Effect of Trench Width and Depth on Film Cooling From Cylindrical Holes Embedded in Trenches," Journal of Turbomachinery, 131(1).
- [23] Waye, S. K., and Bogard, D. G., 2007, "High-Resolution Film Cooling Effectiveness Measurements of Axial Holes Embedded in a Transverse Trench With Various Trench Configurations," Journal of Turbomachinery, 129(2), pp. 294-302.
- [24] Haven, B. A., and Kurosaka, M., 1997, "Kidney and anti-kidney vortices in crossflow jets," Journal of Fluid Mechanics, 352, pp. 27-64.
- [25] Rhee, D. H., Lee, Y. S., and Cho, H. H., "Film Cooling Effectiveness and Heat Transfer of Rectangular-Shaped Film Cooling Holes," Proc. ASME Turbo Expo 2002: Power for Land, Sea, and Air, pp. 21-32.
- [26] Takahashi, H., Nuntadusit, C., Kimoto, H., Ishida, H., Ukai, T., and Takeishi, K., 2006, "Characteristics of Various Film Cooling Jets Injected in a Conduit," Annals of the New York Academy of Sciences, 934(1), pp. 345-352.
- [27] Watson, T. B., Vinton, K. R., Wright, L. M., Crites, D. C., Morris, M. C., and Riahi, A., "Influence of Hole Inlet Geometry on the Film Cooling Effectiveness From Shaped Film Cooling Holes," Proc. ASME Turbo Expo 2019: Turbomachinery Technical Conference and Exposition.
- [28] Ullah, I., Shiau, C.-C., and Han, J.-C., 2019, "Flat plate film cooling with linear and curved round-to-diffusion shaped slots using PSP measurement technique," International Journal of Heat and Mass Transfer, 136, pp. 755-766.

- [29] Yu, Z., Liu, J., Li, C., An, B., and Xu, G., "Experimental Investigation of Film Cooling Performance on Blade Endwall With Diffusion Slot Holes and Stator-Rotor Purge Flow," Proc. ASME Turbo Expo 2020: Turbomachinery Technical Conference and Exposition.
- [30] Zhang, L., and Fox, M., 1999, "Flat plate film cooling measurement using PSP and gas chromatograph techniques," Solar Turbine Inc., San Diego, CA (US).
- [31] Wright, L. M., Gao, Z., Varvel, T. A., and Han, J.-C., 2005, "Assessment of steady state PSP, TSP, and IR measurement techniques for flat plate film cooling," Proc. Heat Transfer Summer Conference, pp. 37-46.
- [32] Charbonnier, D., Ott, P., Jonsson, M., Cottier, F., and Ko'bke, T., "Experimental and Numerical Study of the Thermal Performance of a Film Cooled Turbine Platform," Proc. ASME Turbo Expo 2009: Power for Land, Sea, and Air, pp. 1027-1038.
- [33] Chen, A. F., Li, S.-J., and Han, J.-C., "Film cooling with forward and backward injection for cylindrical and fan-shaped holes using PSP measurement technique," Proc. ASME Turbo Expo 2014: Turbine Technical Conference and Exposition, American Society of Mechanical Engineers Digital Collection.
- [34] Rallabandi, A. P., Grizzle, J., and Han, J.-C., 2011, "Effect of upstream step on flat plate film-cooling effectiveness using PSP," Journal of Turbomachinery, 133(4).
- [35] Kutateladze, S., and Leont'ev, A., 1963, "Film cooling with a turbulent gaseous boundary layer," Thermal Physics of High Temperatures, 1(2), pp. 281-290.
- [36] Natsui, G., Little, Z., Kapat, J. S., Dees, J. E., and Laskowski, G., 2016, "A Detailed Uncertainty Analysis of Adiabatic Film Cooling Effectiveness Measurements Using Pressure-Sensitive Paint," Journal of Turbomachinery, 138(8).
- [37] Dieck, R., Steele, W., and Osolsobe, G., 2005, "Test uncertainty. asme ptc 19.1-2005," American Society of Mechanical Engineers, New York, NY.
- [38] Kline, S., and McClintock, F., 1953, "Analysis of uncertainty in single-sample experiments," Mechanical Engineering, 75(3).
- [39] Burd, S. W., and Simon, T. W., 1999, "Measurements of Discharge Coefficients in Film Cooling," Journal of Turbomachinery, 121(2), pp. 243-248.
- [40] Gritsch, M., Schulz, A., and Wittig, S., 1998, "Discharge Coefficient Measurements of Film-Cooling Holes With Expanded Exits," Journal of Turbomachinery, 120(3), pp. 557-563.

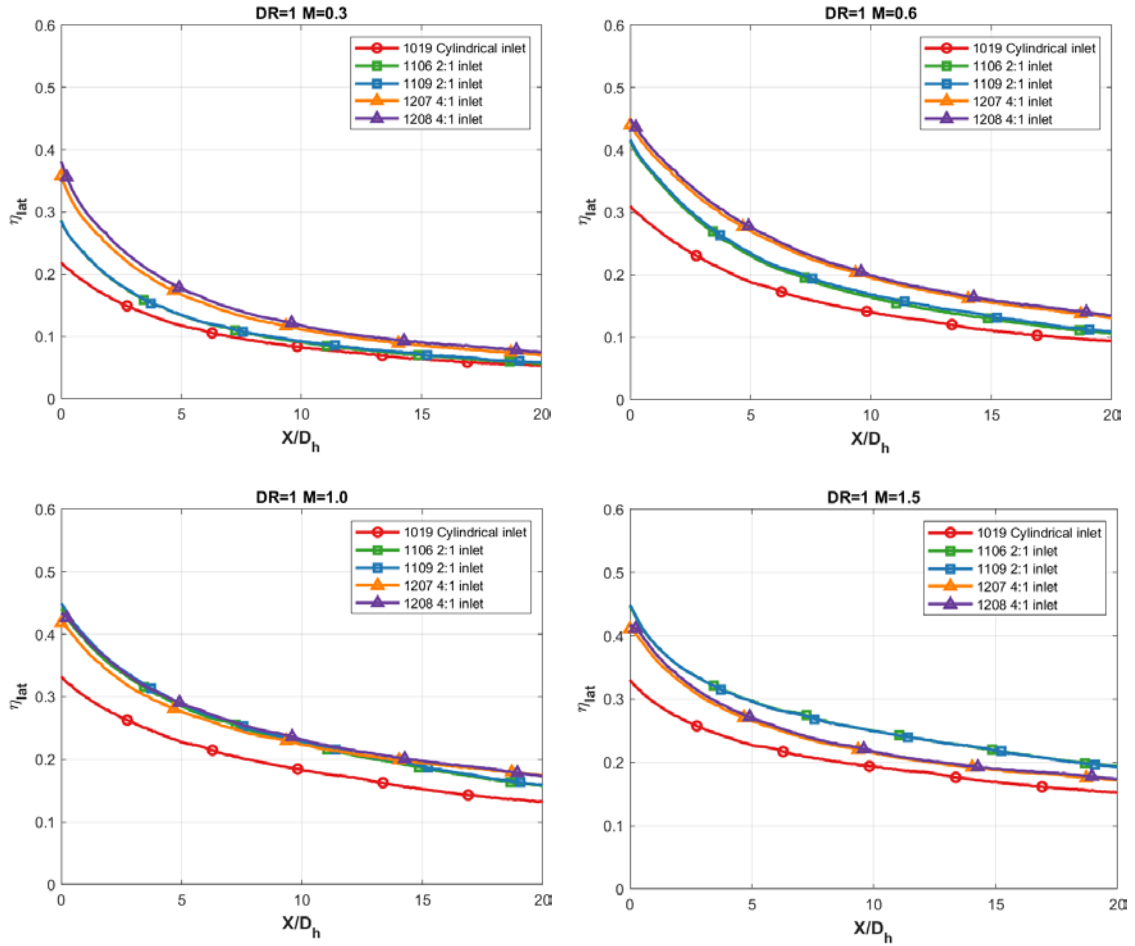
APPENDIX A

LATERAL AVERAGE EFFECTIVENESS PLOTS FOR ALL TESTS

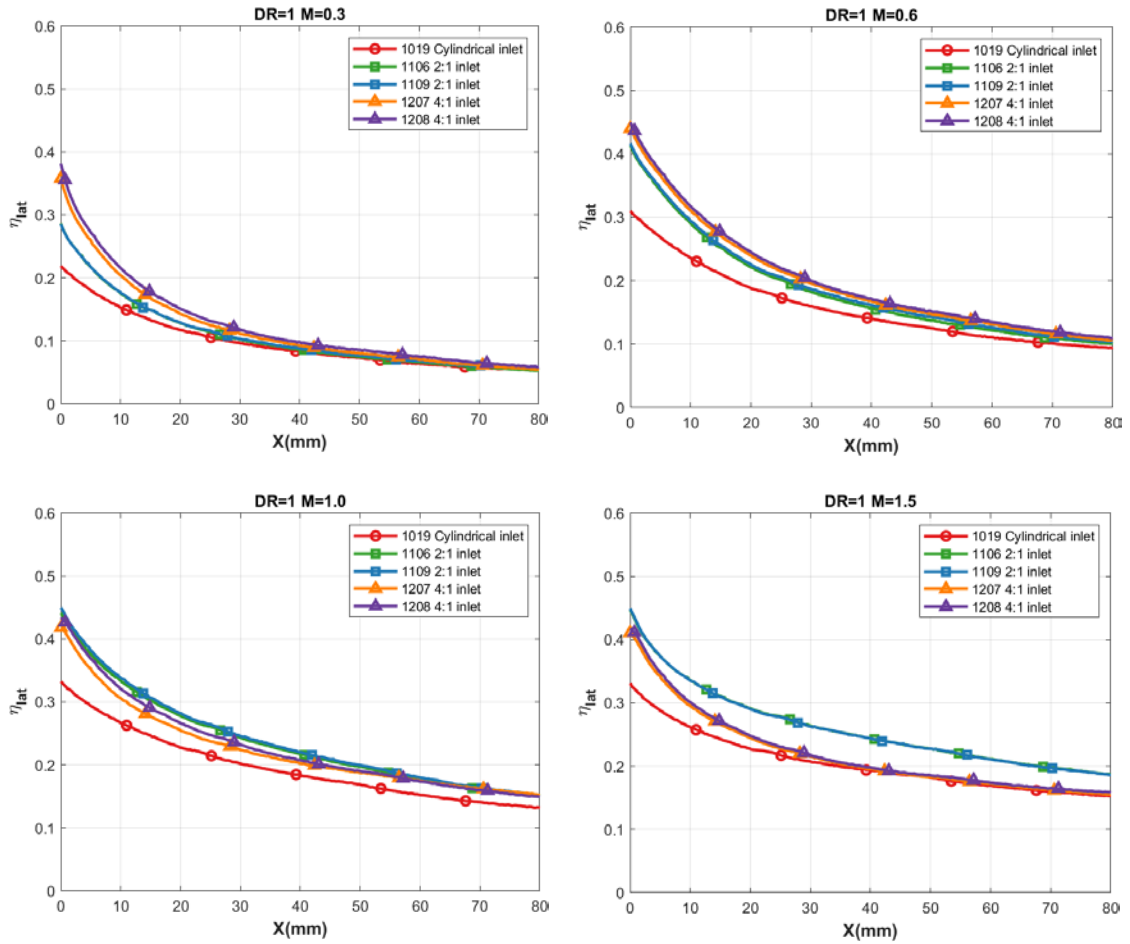
DR=1 Cylindrical holes



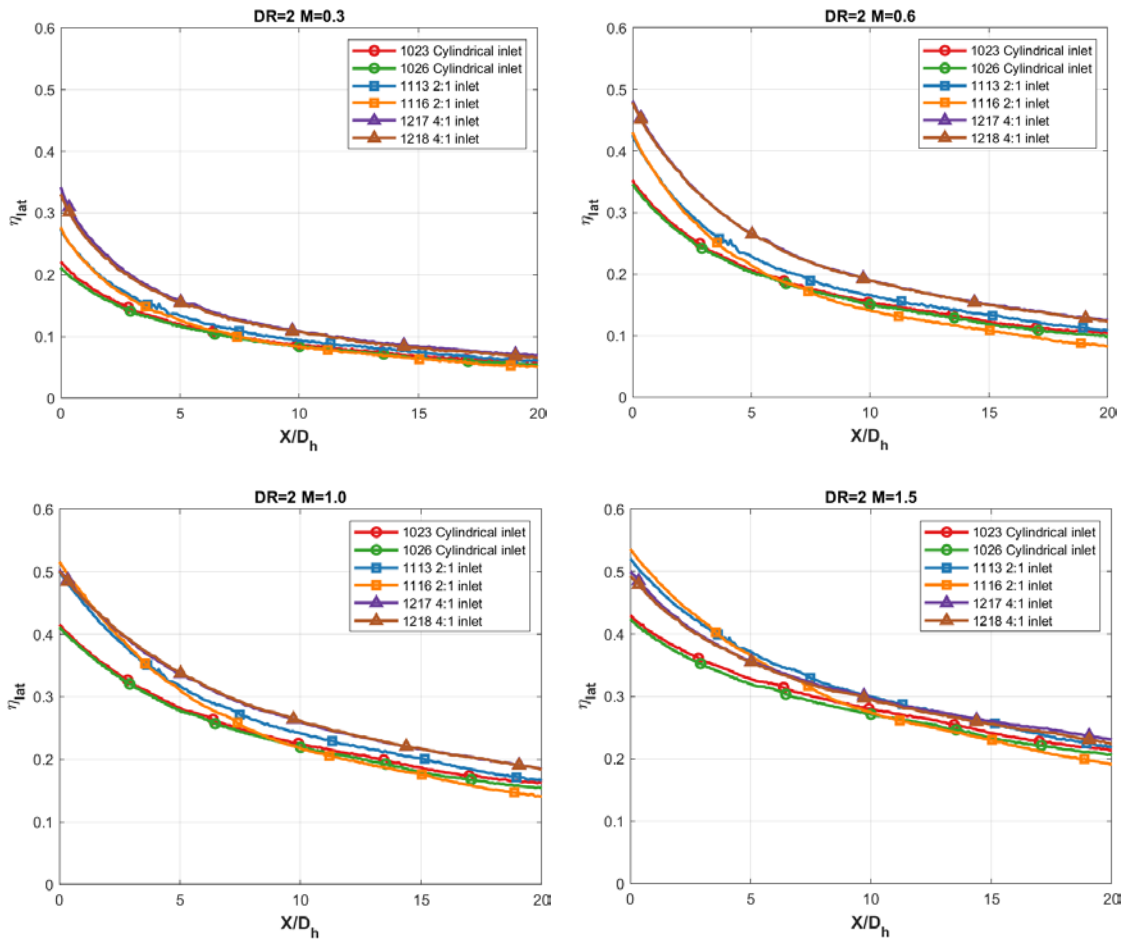
DR=1 Fan shaped holes (Non-dimensional X-axis)



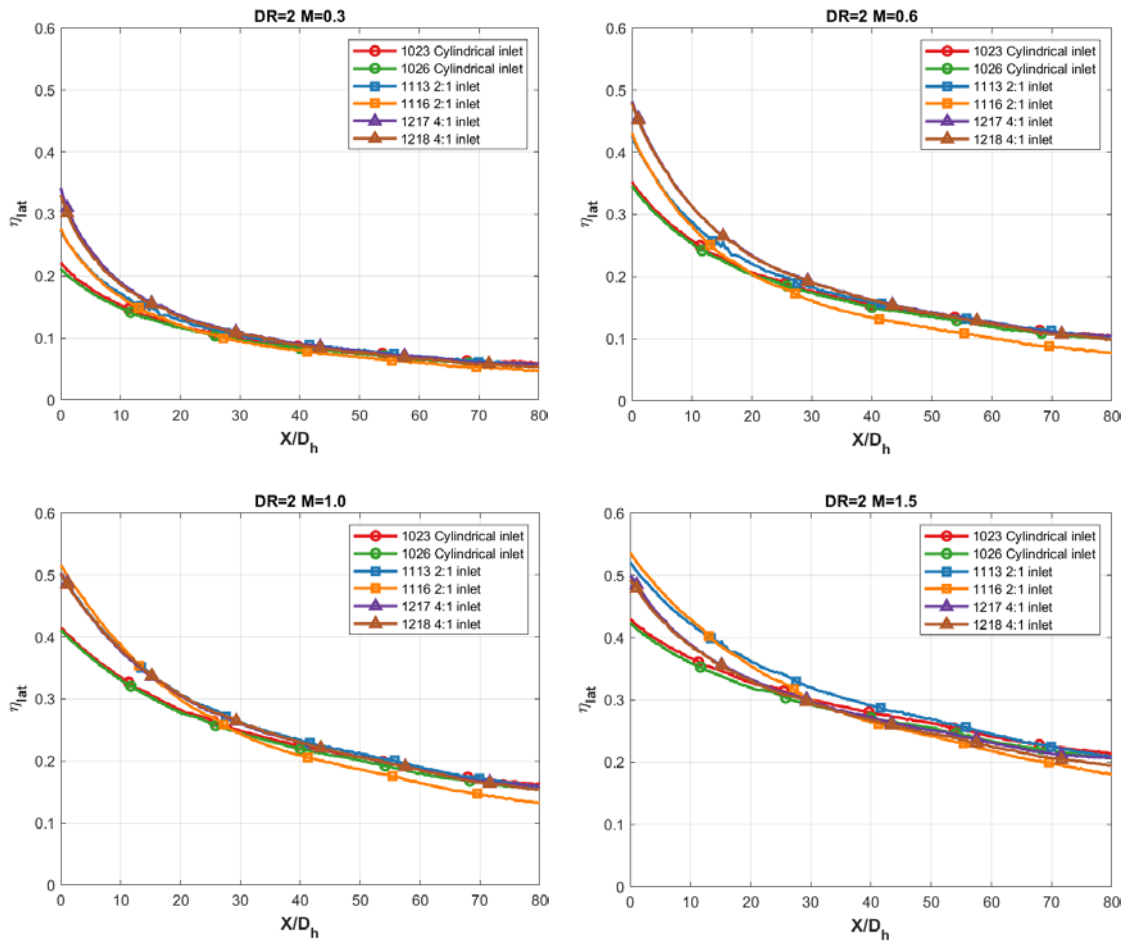
DR=1 Fan shaped holes (Dimensional X-axis)



DR=2 Fan shaped holes (Non-dimensional X-axis)



DR=2 Fan shaped holes (Dimensional X-axis)



APPENDIX B

MATLAB® CODES

MATLAB codes used in this investigation are provided as supplementary files accompanying this thesis.

PSP-extracting Intensity and its standard deviation from Images

```
%% filename:PSP_intensity.m
%% Input
% specify area over which to determine intensity
X0 = 1;    % x-coordinate of starting point
Y0 = 1;    % y-coordinate of starting point

W = 320;   % width of area
H = 240;   % height of area

%measuring the pitch in px and convert it to D_h and D_round
D = 68/24*3.685;
Dround = 68/24*4;

% x (flow) direction offset (start point)
xx = 83;   %431

% y (lateral) direction offset (lateral center)
yy = 121; %24

% specify the file name of the saved images
name = 'blk_';

% specify the file for the intensity output
ofile = 'blk.mat';    % open (create) specified data file

% specify the starting and ending number for the saved images
Start = 1;    % first image number
End = 200;    % last image number

%% Main

% establish the data saving matrices
sum = zeros(H,W);
inten_matrix = zeros(H,W);
n_img=End-Start+1;
Intensity=zeros(H,W,n_img);
Int_std=zeros(H,W);
stdcal=zeros(n_img,1);
```

```

for i = Start:End

    % create a character string with the image number,
    num = sprintf('%04d',i);

    % create a string of the entire image name
    ifile = strcat(name,num, '.tif');

    % read each image file and create a data file (I) with the intensity at each px

    I = imread(ifile);

    I = I(Y0:Y0+H-1,X0:X0+W-1);
    inten = double(I);
    sum = sum + inten;
    Intensity(:, :, i) = double(I);

end

% add the coordinates of the selected area to the data

for ii = 1:W
    xD(ii) = (ii-xx)/D;
    xD_round(ii)=(ii-xx)/Dround;
    for jj = 1:H

        yD(jj) = (jj-yy)/D;
        yD_round(jj) = (jj-yy)/Dround;
        inten_matrix(jj, ii) = sum(inten(:,ii)) / (End-Start+1);

    end
end

% calculate stddev of intensity

for m=1:H
    for n=1:W
        for k=1:n_img
            stdcal(k,1)=Intensity(m,n,k);

        end
        Int_std(m,n)=std(stdcal);
    end
end

Int_std_avg=mean2(Int_std);

% save results into the .mat file previously created
save(ofile, 'xD', 'yD','xD','yD_round', 'inten_matrix', 'Int_std', 'Int_std_avg');

```

PSP Calibration

```
%% filename: PSP_calibration.m
clear all
close all
clc

%% Load Intensity Files (Iblk, Iref, and Ical)
blk=load('blk.mat');      % Iblk
ref=load('ref.mat');     % Iref
cal=load('intensity.mat'); % Ical

Ib=blk.inten_matrix;
Iref=ref.inten_matrix;
Ical=cal.inten_matrix;

W=320;
H=240;

%% calculate Iratio

Iratio = (Iref - Ib) ./ (Ical - Ib);

Iratio_avg=mean2(Iratio);

ofile='28.5_IR.mat';
save(ofile,'Iratio','Iratio_avg')
```

PSP Film Cooling Effectiveness Calculation

```
%% filename: effcalc.m
%% eff calculation function
%inputs: calibration constants, blk, air, ref, mix intensity matrices
%         x/D y/D and define an upstream area to check and offset PR
function
[eff,eff_dr,eff_offset,eff_dr_offset,avg_Pr_air_upstream,avg_Pr_mix_upstream,avg_upstream_eff]=effcalc(DR,a_0,a_1,a_2,a_3,blackint,refint,airint,mixint,xD,yD,xD_hi_Prchk,xD_lo_Prchk,yD_hi_Prchk,yD_lo_Prchk)

Iratio_air = (refint - blackint)./(airint - blackint);
Iratio_mix = (refint - blackint)./(mixint - blackint);

Pratio_air = a_3.*(Iratio_air).^3 + a_2.*(Iratio_air).^2 + a_1.*(Iratio_air) + a_0;
Pratio_mix = a_3.*(Iratio_mix).^3 + a_2.*(Iratio_mix).^2 + a_1.*(Iratio_mix) + a_0;

%without offset
eff = (Pratio_air - Pratio_mix)./ Pratio_air;
eff_dr= ones(size(eff))-1./(((Pratio_air./Pratio_mix)-1)*DR+1);

%check upsteram PR
x_hi_Prchk_loc = find(xD >= xD_hi_Prchk, 1);
x_lo_Prchk_loc = find(xD >= xD_lo_Prchk, 1);
y_hi_Prchk_loc = find(yD >= yD_hi_Prchk, 1);
y_lo_Prchk_loc = find(yD >= yD_lo_Prchk, 1);

Prsumair=0;
Prsummix=0;
effsum=0;

for j= y_lo_Prchk_loc : y_hi_Prchk_loc
    for i= x_lo_Prchk_loc : x_hi_Prchk_loc

        Prsumair=Prsumair+Pratio_air(j,i);
        Prsummix=Prsummix+Pratio_mix(j,i);
        effsum=effsum+eff_dr(j,i);
    end
end
avg_Pr_air_upstream=Prsumair/(y_hi_Prchk_loc-y_lo_Prchk_loc+1)/(1+x_hi_Prchk_loc-x_lo_Prchk_loc);
avg_Pr_mix_upstream=Prsummix/(y_hi_Prchk_loc-y_lo_Prchk_loc+1)/(1+x_hi_Prchk_loc-x_lo_Prchk_loc);
avg_upstream_eff = effsum/(y_hi_Prchk_loc-y_lo_Prchk_loc+1)/(1+x_hi_Prchk_loc-x_lo_Prchk_loc);

%offset upstream PR
Pratio_air_offset=Pratio_air-(avg_Pr_air_upstream-1);
Pratio_mix_offset=Pratio_mix-(avg_Pr_mix_upstream-1);

%with offset
eff_offset = (Pratio_air_offset - Pratio_mix_offset)./ Pratio_air_offset;
eff_dr_offset= ones(size(eff))-1./(((Pratio_air_offset./Pratio_mix_offset)-1)*DR+1);

end
```


PSP lateral and area average effectiveness calculation

```
%% filename: lat_avg.m
%% laterally averaged effectiveness calculation function
function [lat_avg]=lat_avg(eff,xD,yD,low_yd,high_yd)

ylow_location = find(yD >= low_yd, 1); %find the indices corresponding
yhigh_location = find(yD >= high_yd, 1); % to the desired later width in terms of Y/D

sum = zeros(1,length(xD));

lat_avg = zeros(1,length(xD));

for jj = 1 : length(xD)

    for ii = ylow_location : yhigh_location

        sum(jj) = sum(jj) + eff(ii,jj); %adding to sum

    end

    lat_avg(jj) = sum(jj) / (yhigh_location - ylow_location + 1); %taking average

end
end

%% filename: area_avg.m
%% area average calculation function
function [effavg]=area_avg(eff,xD,yD,xD_hi_area_avg,xD_lo_area_avg,yD_hi_area_avg,yD_lo_area_avg)

x_hi_area_avg_loc = find(xD >= xD_hi_area_avg, 1);
x_lo_area_avg_loc = find(xD >= xD_lo_area_avg, 1);
y_hi_area_avg_loc = find(yD >= yD_hi_area_avg, 1);
y_lo_area_avg_loc = find(yD >= yD_lo_area_avg, 1);

effsum=0;

for j= y_lo_area_avg_loc : y_hi_area_avg_loc
    for i= x_lo_area_avg_loc : x_hi_area_avg_loc
        effsum=effsum+eff(j,i);
    end
end

effavg=effsum/(x_hi_area_avg_loc-x_lo_area_avg_loc+1)/(y_hi_area_avg_loc-
y_lo_area_avg_loc+1);
end
```

PSP Uncertainty Calculation

```
%% filename:PSP_uncertainty.m
clc
clear all
close all

%% load files

blkintdat=load('blk.mat');

xD=blkintdat.xD;
yD=blkintdat.yD;

blkint=blkintdat.inten_matrix;
blkstd=blkintdat.Int_std;

refintdat=load('ref.mat');

refint=refintdat.inten_matrix;
refstd=refintdat.Int_std;

airintdat=load('air.mat');

airint=airintdat.inten_matrix;
airstd=airintdat.Int_std;

mixintdat=load('mix.mat');

mixint=mixintdat.inten_matrix;
mixstd=mixintdat.Int_std;

%% intensity ratio uncertainty

U_Iratio_air=((refstd./(airint-blkint)).^2+(blkstd.*(refint-airint)./(airint-
blkint).^2).^2+(airstd.*(refint-blkint)./(airint-blkint).^2).^2).^0.5;
U_Iratio_mix=((refstd./(mixint-blkint)).^2+(blkstd.*(refint-mixint)./(mixint-
blkint).^2).^2+(mixstd.*(refint-blkint)./(mixint-blkint).^2).^2).^0.5;

%% Pratio uncertainty
% calibration consts
a_0 =-0.0287;
a_1 =0.6195;
a_2 =0.4723;
a_3 =-0.0602;
Iratio_air = (refint - blkint)./ (airint - blkint);
Iratio_mix = (refint - blkint)./ (mixint - blkint);

Pratio_air = a_3.*(Iratio_air).^3 + a_2.*(Iratio_air).^2 + a_1.*(Iratio_air) + a_0;
Pratio_mix = a_3.*(Iratio_mix).^3 + a_2.*(Iratio_mix).^2 + a_1.*(Iratio_mix) + a_0;

U_Pratio_air=(3.*a_3.*U_Iratio_air.*Iratio_air.^2+2.*a_2.*U_Iratio_air.*Iratio_air+a_1.*U
_Iratio_air);
U_Pratio_mix=(3.*a_3.*U_Iratio_mix.*Iratio_mix.^2+2.*a_2.*U_Iratio_mix.*Iratio_mix+a_1.*U
_Iratio_mix);

%% eta uncertainty
DR=2;
eta=1-1./(((Pratio_air./Pratio_mix)-1).*DR+1);
U_eta_air=Pratio_mix.*DR./((Pratio_mix.*(DR-1)-DR.*Pratio_air).^2).*U_Pratio_air;
U_eta_mix=DR.*Pratio_air./((Pratio_mix.*(DR.*(Pratio_air./Pratio_mix-
1)+1)).^2.*U_Pratio_mix);
U_eta=(U_eta_air.^2+U_eta_mix.^2).^0.5;
U_eta_relative=U_eta./eta.*100;
```